Bioencapsulation in silica sol-gel nano-pores and intrinsic protein fluorescence: ensemble and single molecule

Alexander Malcolm Macmillan

Photophysics Research Group

Department of Physics

University of Strathclyde

Copyright

Dedication

to the memory of my father.

Publications

- J. Karolin, D. Panek, A. M. Macmillan, O. J. Rolinski, and D. J. S. Birch, "Fluorescence Biosensing in Nanopores", accepted to IEEE August 2009.

- A. M. Macmillan, J. Karolin, D. Panek, C. D. McGuinness, J. C. Pickup, D. Graham, W. E. Smith and D. J. S. Birch, "Improved biocompatibility of protein encapsulation in sol-gel materials", submitted to Journal of Sol-gel Science and Technology, 2009. 49: P. 380-384

- A. M. Macmillan, C. D. McGuinness, K. Sagoo, D. McLoskey, J. C. Pickup and D.J. S. Birch, "Effect of pH on aqueous phenylalanine studied using a 265-nm pulsed light-emitting diode", Annals of the New York Academy of Sciences., Blackwell Publishing: Oxford. 2008. 1130: p. 300-304.

- J. U. Sutter, A. M. Macmillan, D. J. S. Birch and O. J. Rolinski, "Toward single-metal-ion sensing by Forster resonance energy transfer", Annals of the New York Academy of Sciences., Blackwell Publishing: Oxford. 2008.1130. p. 62-67.

- C. D. McGuinness, A. M. Macmillan, J. Karolin, W. E. Smith, D. Graham, J. C. Pickup and D. J. S. Birch, "Single molecule level detection of allophycocyanin by surface enhanced resonance Raman scattering", Analyst, 2007. 132(7): p. 633-634.

- C. D. McGuinness, C.D., A. M. Macmillan, K. Sagoo, D. McLoskey and D. J. S. Birch, "Excitation of fluorescence decay using a 265 nm pulsed light-emitting diode: Evidence for aqueous phenylalanine rotamers", Applied Physics Letters, 2006. 89(6), 063901: p. 1-3

Conference contributions

- A. M. Macmillan, J. Karolin, C. D. McGuinness, D, Pánek, J. C. Pickup and D. J.S. Birch, Single-molecule fluorescence detection of allophycocyanin (APC) entrapped in a silica sol-gel glass under physiological conditions, Poster presentation: MAF 10, Salzburg 9 - 12 September 2007.

- A. M. Macmillan, C. D. McGuinness, K. Sagoo, D. McLoskey, J. C. Pickup and D. J.S. Birch, Aqueous phenylalanine rotamer model using a 265 nm pulsed light-emitting diode, Poster presentation: MAF 10, Salzburg 9 - 12 September 2007.

- J. U. Sutter, A. M. Macmillan, D. J.S. Birch and O. Rolinski, Towards single metal ion sensing by Forster resonance energy transfer, Poster presentation: MAF 10, Salzburg 9 - 12 September 2007.

- A. M. Macmillan, D. Panek, J. Karolin, C. D. McGuinness, J. C. Pickup and D. J.S. Birch, Replicating nature's building blocks in silica sol-gel nano-pores, Poster presentation: SUPA annual meeting, June 13, 2007, University of Edinburgh

- A. M. Macmillan, C. D. McGuinness, K. Sagoo, D. McLoskey, J. C. Pickup and D. J.S. Birch, Excitation of fluorescence decay using a 265 nm pulsed light-emitting diode: Aqueous rotamers of the amino acid L-phenylalanine, Poster presentation: Medical Photonics Workshop, 29th-30th Jan 2007, University of St Andrews

Acknowledgements

Firstly, I would like to thank my supervisor Professor David Birch, for his help, guidance and encouragement throughout the duration of this PhD, and indeed for giving me the opportunity to undertake this project.

I would also like to give a very special thanks to Dr Jan Karolin, again for his support, guidance and discussion and for providing his time in helping with this project.

I am indebted to John Revie in mechanical support and to John Broadfoot in electronics support. Their advice and their technical expertise were invaluable

I would also like to thank David McLoskey at Horiba Jobin Yvon IBH Ltd., Glasgow, who provided the UV light sources for the research discussed in this thesis.

I would like to give special thanks to both past and present colleagues in the Photophysics Research Group for many valuable conversations, and technical expertise, and for making my time in the group very enjoyable.

Thanks are extended to the Engineering and Physical Sciences Research Council (EPSRC) for the tenure of the research studentship.

I would like to give a very special thank you to Stephanie O Connor, for her continued support and encouragement over the years. I would also like to extend a thank you to Murdo, Janette, and Lynsey for their continued support and encouragement.

My greatest debt is to my parents who have supported me endlessly throughout my university education, and with whom none of this would be possible.

Abstract

The ability to measure and understand protein fluorescence depends on the development of light sources which can excite the intrinsic aromatic amino acids, tryptophan, tyrosine, and phenylalanine. In recent years the time-resolved study of protein fluorescence has been limited to the excitation of tryptophan and tyrosine. The availability of the shorter wavelength, 265nm light source, allows for the excitation of phenylalanine which until recently has been limited. In this thesis the direct excitation of phenylalanine is demonstrated, using pulsed light emitting diodes, and the bi-exponential nature of its fluorescence decay is investigated, and the effect of pH on the fluorescence lifetimes.

One of the major difficulties with the study of proteins is the lack of immobilisation techniques for the study of proteins at the single-molecule level, which provide little perturbation of the protein. To try to achieve this, the fabrication of novel molecular nanoenvironments, based on sol-gel techniques, which allow control and enhancement of protein fluorescence has been developed. In this thesis the application of sol-gel techniques is demonstrated for the environment sensitive trimeric form of allophycocyanin (APC) at both the ensemble and single-molecule level. The optimisation of the sol-gel technique as a generic approach to entrapment of proteins was developed using the environment sensitive probe 6-propionyl-2-(N,N-dimethylamino)naphthalene (PRODAN), which enabled monitoring of the hydrolysis and methanol removal stage of the process.

For earlier diagnosis, ultra sensitive monitoring and breakthroughs in understanding the causes of many diseases, we urgently need to develop clinical single molecule sensing. Downstream, this might be accomplished by means of the fluorescence nanosecond/nanometre microscopy of single biomacromolecules.

Table of Contents

1

1. Introduction

Fluorescence has found many applications in analytical science due to its sensitivity, and its ability to detect fluorophores at concentrations of a few parts per billion. Fluorescence occurs typically on the picosecond to nanosecond time scale, and is therefore comparable to the time scales of many molecular processes. Fluorescence lifetime spectroscopy has found application in many fundamental areas of science including the investigation of proteins, membranes, inorganic crystals, semiconductors, and low dimensional structures [1].

Proteins display intrinsic fluorescence in the near ultraviolet region due to the presence of aromatic amino acids, namely tryptophan, tyrosine, and phenylalanine. These natural markers allow for the study and monitoring of conformational changes within proteins, which are reflected by shifts in fluorescence spectra, changes in quantum yield, and alterations in fluorescence decay kinetics. For example intrinsic tryptophan fluorescence has been used to monitor the complex formation of the protein human serum albumin (HSA) with two flavanoids, quercetin and morin [2].

The ability to measure and understand protein fluorescence depends on the development of light sources which can excite the intrinsic aromatic amino acids, tryptophan, tyrosine, and phenylalanine. In recent years the time-resolved study of protein fluorescence has been

limited to the excitation of tryptophan and tyrosine. The availability of the shorter wavelength, 265nm light source, allows for the excitation of phenylalanine which until recently has been limited. In this thesis the direct excitation of phenylalanine is demonstrated, using pulsed light emitting diodes, and the bi-exponential nature of its fluorescence decay is investigated, and the effect of pH on the fluorescence lifetimes.

The immobilisation of proteins is crucial in several applications such as separation science, bioreactor design, and the development of selective chemical and biochemical sensors. Hydrated silica sol gels can be applied to the encapsulation of proteins whilst retaining biological function. These materials offer the advantage of being optically transparent making them ideally suited to the application of sensors based on changes in absorbance or fluorescence [3]. However, there is still relatively little known about the local environments within the nano-pores where the proteins are encapsulated. Therefore, it is important that methods be developed to allow for investigation of the composition of the internal pore liquid and also to ensure that methanol, which denatures proteins, is removed in the early stages of the synthesis.

The interest in single molecule protein studies has been rapidly growing over the last few years. While ensemble measurements allowed for an overview of protein changes, the ability to monitor a single protein molecule allows for recording of individual changes in protein conformation and recording of the time processes involved. The ability to monitor such changes in single-proteins may lead to further understanding of protein dynamics, with possible enhanced understanding of protein mis-folding. This has implications to diseases such as prion diseases, diabetes and cancer, which share the pathological feature of aggregated misfolded protein deposits [4].

At present, diagnosis and monitoring in clinical biochemistry is based on measurement of average concentration, molecular form and bioactivity of ensembles of proteins and other

macromolecules, thereby losing sensitivity and the ability to discriminate amongst the range and pattern of biomolecular diversity in pathology.

For earlier diagnosis, ultra sensitive monitoring and breakthroughs in understanding the causes of many diseases, we urgently need to develop clinical single molecule sensing. This might be accomplished by means of the fluorescence nanosecond/nanometre microscopy of single biomacromolecules.

One of the major difficulties with the study of proteins is the lack of immobilisation techniques [5] for the study of proteins at the single-molecule level, which provide little perturbation of the protein. In order to try and achieve immobilised and unperturbed proteins, down to single molecule, the fabrication of novel molecular nanoenvironments, based on sol-gel techniques, which allow control and enhancement of protein fluorescence has been developed.

With the continuing development of light sources and surface plasmon enhancement techniques, the ability to study single proteins through their intrinsic aromatic acid residues is not unrealistic. The ability to utilise naturally occurring fluorescence in proteins eliminates any intrusion by dye labelling.

The work presented in this thesis describes the development and application of silica sol-gels and how in turn this matrix can be applied to the immobilisation of environment sensitive proteins for single-protein fluorescence measurement. The application of chemical scavengers to the removal of oxygen from both solution and the internal sol-gel pore liquid is investigated as a method for stabilising fluorophores. While not necessary for ensemble measurements, the removal of oxygen would allow for easier measurement of single-molecules by enhancing there stability by limiting intersystem crossing. While in

the triplet state molecules are susceptible to photo-oxidation which results in permanent photodestruction of the molecule. Also, the application of ultra-violet light emitting diodes to the study of the aromatic amino acid phenylalanine is presented. The rotamer model is discussed and applied to phenylalanine for the first time. Although the phenylalanine chromophore in proteins is not expected to behave identically to the results reported in this thesis, the two environments will be more similar than those between the gas and solution phases, from which we can still draw useful comparisons. Although phenylalanine fluorescence is difficult to detect in most proteins because of its low quantum yield and resonance energy transfer from phenylalanine to tyrosine and tryptophan, the ability to directly excite the chromophore may well take protein photophysics in new directions, for example, by making use of this resonance energy transfer or by observing phenylalanine fluorescence directly in specific proteins where resonance energy transfer to other amino acids is inefficient.

2

2. Background principles

2.1 Luminescence

Luminescence describes the emission of light from an electronically excited state. Luminescence can be divided into two categories, fluorescence and phosphorescence, which categorise the light emission.

Fluorescence occurs when molecules are radiatively de-excited, from a singlet state, after initial absorbance of photons. In an excited singlet state, an electron in the excited orbital is spin paired to an electron of opposite spin in the ground-state orbital. The transition from excited state to ground state, with associated emission of light (fluorescence), is therefore described as being spin allowed as determined by quantum mechanical laws. The phenomenon was first described by Sir John Frederick William Herschel in 1845, after he observed the emission of blue light as a result of ultra-violet (UV, sunlight) excitation of quinine in tonic water [6].

Phosphorescence occurs when molecules radiatively de-excited, from a triplet state, after initial absorbance of photons. In an excited triplet state, an electron in the excited orbital is spin paired to an electron of same spin in the ground-state orbital. The transition from excited state to ground state is therefore described as being spin forbidden.

The electronic state and transitions between states of a molecule can be most readily illustrated by a Jablonski diagram, as shown in figure. 2.1. The ground electronic state is represented by S_0 with S_1, S_2 etc representing higher energy singlet states and T_1, T_2 representing triplet states. The states are arranged vertically by energy, with a transition from S_0 to S_1 associated with the absorbance of energy and the inverse with the depopulation by radiative (fluorescence) or non-radiative mechanism. Electronic states are grouped horizontally as determined by spin multiplicity. Each electronic level are further divided into vibrational and rotational energy levels. Therefore, the total energy of (E) is the sum of the electronic (E_e), vibrational (E_v), and rotational energies (E_r). Typical wavenumber differences between electronic, vibrational, and rotational energy levels are 30,000 cm^{-1}, 1,000 cm^{-1}, and 10 cm^{-1} respectively [7]. The wavenumber can be related to energy via equation 2.1.

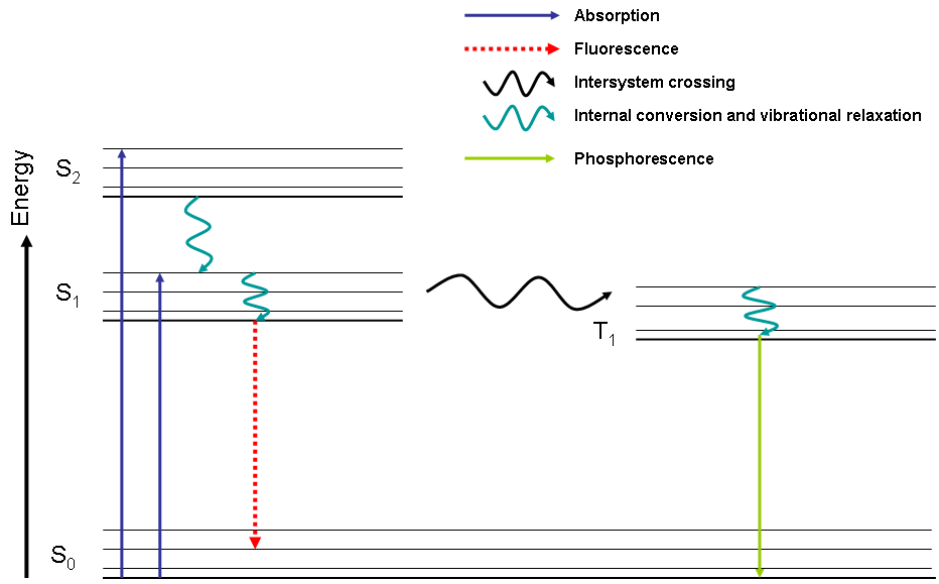

Figure 2.1 Jablonski diagram indicating electronic and vibrational energy levels and transitions.

When a molecule absorbs a photon, it is usually excited to a higher vibrational energy level within an excited state, the process normally occurring in 10^{-15} seconds. The transitions between states are depicted as vertical lines in figure 2.1, to illustrate the instantaneous

nature of the transition. The molecule rapidly relaxes to the lowest vibrational level, in a process called internal conversion (loss of vibrational energy, ~10^{-12} second timescales), prior to radiative relaxation to the ground state energy level. Typically, internal conversion results in energy of emission being of less magnitude that the absorbance energy, and therefore the fluorescence emission is red shifted from that of the absorption spectrum. This is known as the "Stokes shift" and was first described by Sir George Gabriel Stokes in 1852 [8]. For most molecules fluorescence occurs exclusively from the lowest excited state, and therefore the fluorescence spectrum is the same irrespective of the excitation wavelength, as described by Kasha's Rule [9]. The radiative transition from S_1 to S_0, is a slower process with respect to internal conversion and typically occurs on a nanosecond timescale (10^{-9} seconds) and is called fluorescence.

2.2 Excitation of electronic states

2.2.1 Absorption

Absorption of electromagnetic radiation is the way by which the energy of a photon is taken up by matter, typically the electrons of an atom.

When a molecule absorbs electromagnetic radiation, its resultant energy has increased by an amount of equal magnitude to the absorbed photon. The energy of the photon being derived from the Nobel Prize winning Einstein equation, as shown in equation 2.1.

$$E = h\nu = hc/\lambda = \hbar ck \qquad (2.1)$$

Where E is the photon energy, h is Planck's constant (6.626 x 10^{-34} J s^{-1}), ν is the frequency (Hz), c is the speed of light (m s^{-1}), λ is the wavelength (nm), and k is the wavenumber (cm^{-1}).

The wavenumber (k) is calculated from the wavelength (λ) via equation 2.2.

$$\mathbf{k = 2\pi/\lambda} \qquad (2.2)$$

The Beer-Lambert law is the linear relationship between absorbance and concentration of an absorbing species. When working in concentration units of molarity, the Beer-Lambert law is written as:

$$A = \epsilon c l \qquad (2.3)$$

Where A is the measured absorbance, ϵ is a wavelength-dependent absorption coefficient (M^{-1} cm^{-1}), c is the analyte concentration (mol L^{-1}), and l is the path length (cm).

2.2.2 Absorption measurement

The absorbance can be measured in terms of change of magnitude between incident light and transmitted light. Where transmitted light is defined as:

$$T = I / I_0 \qquad (2.4)$$

Where I_0 is the intensity of monochromatic radiation entering the sample and I is the intensity of radiation leaving the sample.

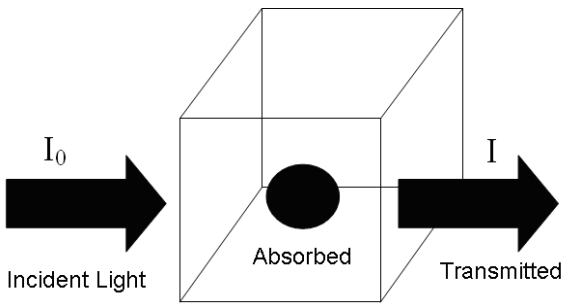

Figure 2.2 Illustration of light transmittance and absorbance

And absorbance can be defined in terms of transmittance as:

$$A = - \log_{10} I / I_0 = \epsilon c l \qquad (2.5)$$

2.3 Fluorescence parameters

2.3.1 Quantum yield

The fluorescence quantum yield can be described as the number of photons emitted relative to the number of photons absorbed. If the rate of radiationless decay is much smaller than the rate of radiative decay, quantum yields close to unity may be approached. Such quantum yields are displayed by Rhodamine dyes, (Rhodamine 123 has a quantum yield of 0.9), and this is observed by their bright emission. The quantum yield is given by:

$$\Phi = k_r / (k_r + k_{nr}) \qquad (2.6)$$

Where Φ is the quantum yield, k_r is the rate of radiative decay, and k_{nr} is the rate of radiationless decay.

It can be seen from equation 2.6 that the energy yield of fluorescence is always less than unity.

Non-radiative decay describes all mechanisms by which excited state decay occurs without photon emission. Such mechanisms include dynamic collisional quenching, near-field dipole-dipole interaction (or resonance energy transfer), internal conversion and inter-system crossing.

2.3.2 Fluorescence quenching.

Fluorescence quenching refers to any process which decreases the fluorescence intensity. There are a number of molecular interactions which can result in quenching, namely excited state reactions, molecular rearrangements, energy transfer and collisional quenching. The most commonly observed quenching mechanism is collisional quenching, and this mechanism will be discussed in detail in this chapter. One of the best known collisional quenchers is molecular oxygen, which quenches almost all known fluorophores [10,11].

Collisional (or dynamic) quenching describes the attenuation of fluorescence by collisional encounters between a fluorophore and the quencher, and is described by the Stern-Volmer equation (2.7).

$$F_0/F = 1 + k_Q \tau_0 [Q] = 1 + K_D [Q] \qquad (2.7)$$

Where F_0 and F are the fluorescence intensities in the absence and presence of a quencher respectively, k_Q is the biomolecular quenching constant, τ_0 in the fluorescence lifetime in the absence of quencher, and is the concentration of the quencher. The Stern-Volmer quenching constant $K_D = k_Q \tau_0$.

Quenching is often represented by a plot of F_0/F versus. The F_0/F data is expected to be linearly dependent on the concentration of the quencher.

In terms of fluorescence lifetime, the Stern-Volmer equation can be written as (2.8):

$$\tau_0/\tau = F_0/F = 1 + K_D [Q] \qquad (2.8)$$

Where τ_0, and τ, are the fluorescence lifetimes, in the absence and presence of a quencher respectively.

2.4 Time-domain fluorescence

Fluorescence measurements in the time-domain (fluorometry) provide considerably more information content with regard to rates and hence kinetics of inter- and intramolecular processes in comparison to the information provided by steady-state fluorescence measurement (fluorimetry) [12]. This is due to steady-state spectra providing average information over the whole scan whilst fluorescence emission itself occurs on a nanosecond time-scale.

Fluorescence lifetime measurements can be applied to the determination of a fluorescent molecules local environment e.g. pH, viscosity, temperature, polarity [13]. Also, information regarding the shape and size of molecules [14] and of inter-molecular distances [15] can be determined using fluorescence lifetime measurement . The use of the fluorescent molecule as a probe for local environment can be illustrated by considering the dependence of the molecular fluorescence lifetime τ_M on the rates of competing decay pathways as shown in equation 2.9.

$$\tau_M = 1/(k_r + k_{nr}) = 1/ k_M \qquad (2.9)$$

Where k_r is the radiative rate parameter (in s^{-1}), and k_{nr} is the non-radiative rate parameter and k_M the total decay rate. Both k_r and k_{nr} can be directly dependant on environmental factors such as temperature, refractive index, and polarity [12].

There are two techniques for the measurement of fluorescence lifetime, namely phase and pulse fluorometry. In the time domain, a short pulse of light excites the sample, and the subsequent fluorescence emission is recorded as a function of time. This usually occurs on the nanosecond timescale. In the frequency domain, the sample is excited by a modulated source of light at a frequency ω. The fluorescence emitted by the sample has a similar waveform, but is modulated and phase-shifted from the excitation curve. Both modulation (M) and phase-shift

(φ) are determined by the lifetime of the sample emission; that lifetime (τ) can be calculated from the observed modulation and phase-shift. The relevant equations are shown in 2.10 and 2.11.

$$\text{Tan } \varphi = - \omega\tau \qquad (2.10)$$

$$M = 1/ (1 + \omega^2\tau^2)^{1/2} \qquad (2.11)$$

In the time-domain the fluorescent sample is excited by a pulse of light. The width of the pulse is as small as possible, and considerably shorter in comparison to the sample decay time τ. The fluorescence lifetime can be determined experimentally by measuring the time taken for the fluorescence intensity to fall to 1/e of the initial intensity following excitation by a δ-function pulse, as illustrated by figure 2.3.

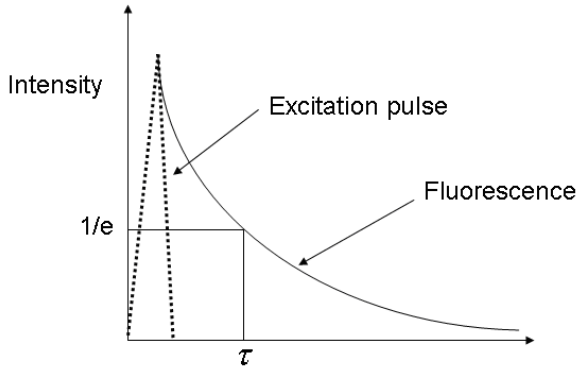

Figure 2.3. Schematic showing excitation pulse (⋯⋯) and fluorescence decay (—). The fluorescence lifetime (τ) is determined by measuring time taken for fluorescence intensity to fall to 1/e after excitation.

The depopulation of the S_1 state can be, in its simplest case, modelled by a mono-exponential decay, as shown by equation 2.12.

$$\frac{d[M^*]}{dt} = -\frac{[M^*]}{\tau} \qquad (2.12)$$

Which upon integration gives (2.13):

$$[M^*] = [M^*]_0 \, e^{(-t/\tau)} \qquad (2.13)$$

Where [M*] is the excited state concentration at time t, and $[M^*]_0$ is the excited state concentration at time t=0, and τ is the molecular fluorescence lifetime.

2.4.1 Time -correlated single-photon counting (TCSPC)

The application of the time-correlated single-photon counting technique to the measurement of fluorescence lifetime was first described by Bollinger and Thomas in 1961, where they demonstrated the measurement of the scintillation response for various crystals using gamma, neutron and alpha excitation [16]. The basic principals described by Bollinger and Thomas remain the same, however excitation is now normally achieved by optical excitation [12].

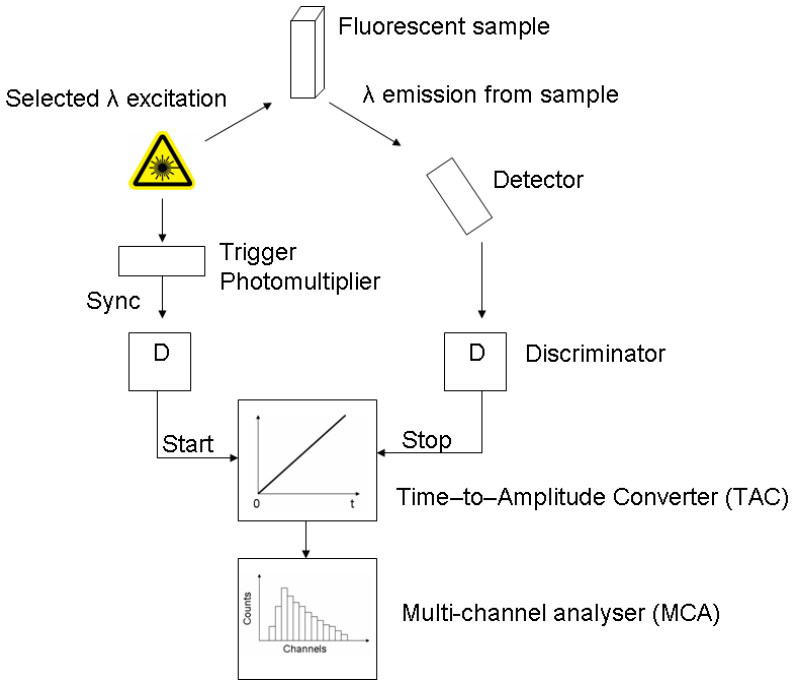

Figure 2.4. Generic layout for TCSPC.

2.4.2 Time-Correlated Single-Photon-Counting fluorometer.

A pulsed light source, such as a light emitting diode (LED), mode locked laser, or more traditionally a coaxial flashlamp is used to excite the sample repeatedly. The fluorescence generated by excitation of the sample is observed by a detector, such as a photomultiplier tube, and more recently an avalanche photodiode (APD). As an excitation pulse is generated a synchronization or "start" pulse triggers the charging of a capacitor in the Time-to-Amplitude Converter (TAC), which in turn produces an analogue voltage, or time-to-pulse height conversion (TPHC), which is proportional to elapsed time between stop and start signals. The stop signal being generated by the detection of the first photon generated by sample emission.

The multi-channel analyser (MCA) records repetitive start-stop signals of the single-photon events from the TAC, to generate a histogram of photon counts as a function of time channel units. The decay parameters are then extracted using on-line data analysis of the histogram using numerical and statistical procedures.

2.4.3 Data analysis: Reconvolution and least squares method

The TCSPC technique is designed with the overall aim of determining the fluorescence lifetime. Determination of the kinetic parameters requires the application of statistical methods of data analysis.

A convolution is an integral that expresses the amount of overlap of one function as it is shifted over another function.

The measured excitation pulse is broader in comparison to the optical pulse due to timing jitter introduced by the TCSPC components. The main sources of this broadening are the single-photon timing detector such as a photomultiplier, the timing electronics such as the constant fraction discriminator, and optical components such as the monochromator [12,17,18]. The instrumental response is determined by measuring the response from a scattering medium such as silica solution. The measured instrumental full width half maximum (FWHM) Δt_m can be given by equation 2.14:

$$\Delta t_m \approx [(\Delta t_e)^2 + \sum_i (\Delta t_i)^2]^{1/2} \qquad (2.14)$$

Where the timing jitter introduced by the *ith* component in the TCSPC instrument is given by Δt_i and the FWHM of the excitation pulse is give by Δt_e.

A non δ-function instrument response requires the deconvolution of the fluorescence response function with the instrument response in order to recover the fluorescence lifetime. The experimental measurement of *P(t)* over *i* channels of data allows for the convoluted form of *F(t)* to be obtained [12,18]. The instrument response and fluorescence decay convolution can be expressed as follows:

$$F(t) = \int_0^t P(t')i(t-t')dt' \qquad (2.15)$$

Where *F(t)* is the fluorescence decay, *P(t)* is the instrumental response, and *i(t)* the theoretical fluorescence response function which would be derived from δ-function excitation.

2.4.4 Least-squares method

Least squares can be interpreted as a method of fitting data [19]. In terms of fluorescence decay the fit parameters (τ etc) are given an initial value and the fluorescence decay profile *F'(t)* is calculated by convolution of the above parameters [12].

The chi-squared (χ^2) value represents the "goodness of fit" between the actual deviation (the difference between the fluorescence decay value *(Y(i))* and the fitting function value *(Fy(i))*, and the expected deviation, which is the deviation expected due to statistical noise, as shown in equation 2.16.

$$\chi^2 = \sum_{\text{data}} \left[\frac{\mathrm{Y}(i) - \mathrm{F_Y}(i)}{\sigma(i)} \right]^2 = \sum_{\text{data}} [W(i)]^2 \qquad (2.16)$$

Equation 2.16 can be rewritten as:

$$\chi^2 = \sum_{data} \left[\frac{\text{actual deviation}}{\text{expected deviation}} \right]^2 \qquad (2.17)$$

Where the *W(i)* term is the weighted residual, and $\sigma(i)$ is the statistical uncertainty of the *ith* data point.

If the correct fitting function is applied the actual and expected deviation should be close to unity, giving:

$$\chi^2 = \textbf{Number of data points (N)} \qquad (2.18)$$

However, the expected deviation is a statistical expectation, and as a result is an average value. Also, the number of fitted parameters, υ, must be taken into account, giving:

$$\chi_N^2 = \frac{\chi^2}{(N-\upsilon)} \qquad (2.19)$$

Where, (N-υ) is the number of degrees of freedom, and should be used in place of N.

A χ^2 value of 1 represents a good fit, although a value of χ^2 between 1 and 1.2 is acceptable. A χ^2 value > 1.2 suggest that an inappropriate model is being used to describe the data, or systematic error is present.

Weighted residuals, as shown in figure 2.5, are an important means of assessing the goodness of fit as they show where misfits occur. Normalisation of the weighted residuals compensates for the varying data precision within the data set and between data sets. The deviations are expressed in a statistically meaningful way in terms of the standard deviations of the associated data noise, and the relationship between residuals and χ^2 is straightforward.

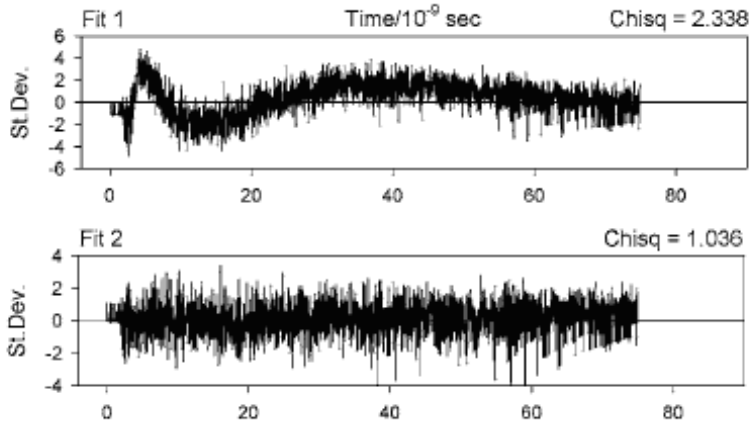

2.5. Weighted residuals for correct model and incorrect fitting.

2.5 Confocal microscopy

The basic concept of confocal microscopy was first introduced by Marvin Minsky in the mid 1950s [20]. However, due to a lack of powerful light sources, at the time, the concept went relatively unnoticed. The confocal microscope found renewed interest in the 1990s, due to the advances in optics, more stable and powerful lasers, high-throughput fibre optics, and improved detectors. These advances resulted in the application of confocal microscopes to the routine investigation of molecules, cells, and living tissues that previously were not possible.

Confocal microscopy is a technique which allows for the construction of three dimensional images and improved resolution compared with widefield microscopy. The improvement in resolution is due to the presence of a pinhole aperture placed in front of the detector which ensures that only light within the focal plane is detected.

2.5.1 Principles of confocal microscopy

Coherent light is emitted from a laser (excitation source) and then passes through a pinhole aperture which is situated in a conjugate plane (confocal) with a scanning point on the specimen. The laser light is reflected, by a dichroic mirror and scanned across the sample in a defined focal plane. The fluorescence emission, which is in the same focal plane, is transmitted through the dichroic mirror and focused at the detector pinhole aperture, as illustrated in figure 2.6. The ability of a dichroic mirror to reflect the excitation light and allow transmission of the sample fluorescence allows for the excitation and resultant collection of fluorescence to be collected through the same objective.

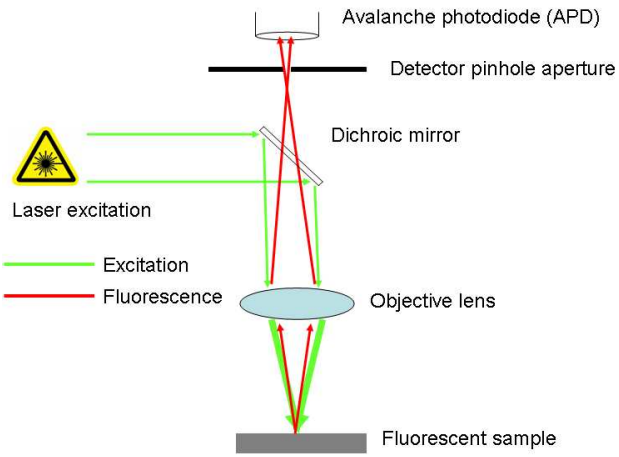

Figure 2.6. Principles of a confocal microscope.

This objective is responsible for the magnification of the substrate and the focusing of the laser beam. The numerical aperture is a measure of the optical resolution and the light sensitivity of the lens and is defined as follows (2.20):

$$NA = n \sin \theta \qquad (2.20)$$

Where, NA is the numerical aperture, n the refractive index of the medium between lens and sample, and θ half the angle subtended by the lens at its focus.

The detector pinhole aperture permits only light that is from the focal volume and rejects any light occurring from above or below the focal plane. As a result of the decrease in focal volume, as compared with other microscopy techniques (wide-field), the signal-to-noise (S/N) ratio is greatly improved with the confocal technique.

The low light levels passing through the detector pinhole aperture necessitate the use of highly sensitive photon detectors. For single molecule measurement low noise level is also a requirement of the detector. There are three detectors which are commonly used for confocal microscopy, photomultiplier tubes (PMT), charged coupled devices (CCD) and avalanche photodiodes (APD) [21].

There are two methods of obtaining images from a confocal microscope, the first is termed confocal scanning laser microscopy (CSLM), in this method the sample is fixed in place and the laser beam scanned across the sample [22]. The second method involves the laser beam being fixed in place and the sample being moved [23]. The results presented in this thesis were recorded using the latter method with the sample moved by a piezoelectrical driven stage.

In confocal microscopy the laser excitation source is focused by a lens system to a very small spot at the focal plane. The size of the illumination point ranges from approximately 0.25 to 0.8 micrometers in diameter (depending upon the objective numerical aperture) and 0.5 to 1.5 micrometers deep at the brightest intensity. The confocal spot size is determined by the microscope design, wavelength of incident laser light, objective characteristics, scanning unit settings, and the type of specimen being imaged [24].

2.6 Silica sol-gels

Interest in sol-gel processing of inorganic materials began in the mid nineteenth century with work published by Ebelman [25,26] on the formation of a glass-like material and then Graham [27] reported on the properties of silicic acid. These early studies reported on the

hydrolysis of tetraethyl orthosilicate (TEOS, $Si(OC_2H_5)$, under acidic conditions. These early experiments resulted in the formation of SiO_2 glass like materials, however the long drying times (~ 1 year) required for these gels, in order to prevent fracturing, resulted in very little technological interest at the time.

Sols are a dispersion of colloid particles in a liquid phase. A gel is an interconnected rigid network of nanometre size pores (typically < 10nm) [28]. The transition from sol to gel occurs when the system can support a stress elastically, and is defined as the gel point (t_g), at which point the network spans the containing vessel.

The sol-gel process is a wet-chemical technique, which forms a rigid network. The complete hydrolysis of an alkoxide precursor, results in the formation of silicic acid ($SiOH_4$). Silicic acid is a highly reactive molecule which rapidly polymerises through condensation reactions. Schematically the reaction can be written for tetramethyl orthosilicate (TMOS):

$$\mathbf{Si(OCH_3)_4 + 4\ H_2O \rightarrow Si(OH)_4 + 4\ CH_3OH\ \ (Hydrolysis\ catalysed\ by\ acid)}$$

$$\mathbf{nSi(OH)_4 \rightarrow porous\ network\ of\ (SiO_2)n + H_2O\ \ (Condensation)} \qquad \mathbf{(2.21)}$$

The tetrafunctional nature of silicic acid can result in the formation of a complex branched polymer. Silicic acid polymerises into discrete particles that in turn aggregate into chains and networks as first recognised by Carmen in 1940 [29]. The rates and formation of sol-gels is highly dependent on pH, temperature, solvent, and SiO_2 concentration [28,30].

A generalised depiction of the sol to gel transition is illustrated in figure. 2.7. Nanometre

size particles composed of silica clusters (A), form and aggregate together to form a growing network (B), which spans the containing vessel at a time t_g and then shrinks forming pores (C) [31].

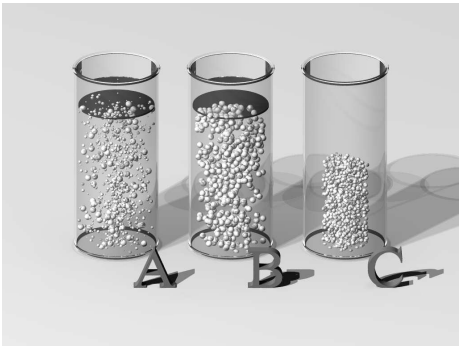

Figure 2.7. Illustration of the sol to gel transition (image reproduced courtesy of Dr Jan Karolin)

In a description presented by Iler [30], he proposed that the polymerisation occurs in three stages.

1. Polymerisation of monomer to form particles.
2. Growth of particles
3. Linking of particles into chains, then networks that extend throughout the liquid medium, increasing its viscosity to form a gel.

The polymerisation can be divided into three approximate pH domains [30]. It can be seen in figure 2.8, that the gel times steadily decrease between pH 2 and pH 7, with the latter pH having the shortest gelation time. It is assumed that above the isoelectric point (pH < 2) the condensation rate is proportional to the OH^- concentration.

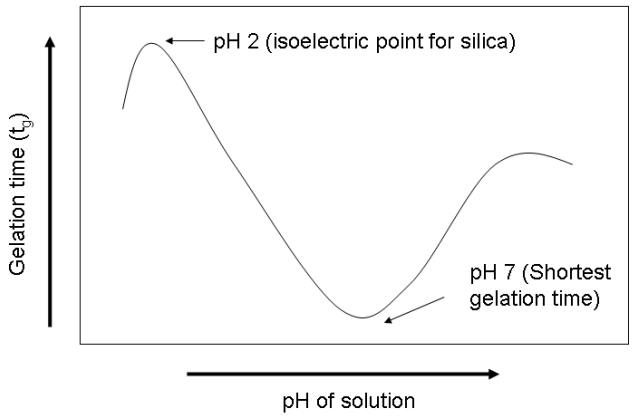

Figure 2.8. Representation of gelation time (t_g) as function of solution pH.

2.6.1 Gel Ageing

After t_g, the properties of the gel continue to change, and this process is termed gel ageing. There are four potential mechanisms which can occur, polymerisation, syneresis, coarsening, and phase transformation. These mechanisms can occur either individually or a combination of two or more.

Polymerisation describes the increased connectivity of the gel network after t_g, as a result of continued condensation reactions in a newly formed gel. Nuclear magnetic resonance (NMR) [32] and Raman spectroscopy [33,34] have shown that condensation reactions can occur long after t_g, due to the large concentration of labile silanol groups. The polycondensation will continue to occur providing that there are silanol groups in close enough proximity to react, resulting in increased crosslinking within the gel network.

Syneresis describes gel shrinkage with expulsion of the pore liquid, and is believed to be caused by the same condensation reactions as produce gelation. The condensation process at the isoelectric point is at its slowest, which suggests that the pore shrinkage is directly

related to the condensation reactions within the gel. The rate of syneresis decreases with time [35]. Shrinkage is ultimately ceased by the remaining repulsive forces.

Coarsening (or Ostwald ripening) is a process of dissolution and reprecipitation driven by differences in solubility between surfaces with different radii of curvature. The result of dissolution-reprecipitation is to reduce the net curvature of the solid phase. Small particles disappear and small pores are filled in, so the interfacial area decreases and the average pore size increases [28]

2.6.2 Drying

The drying of porous materials can be divided into three stages. The first stage involves shrinkage of the gel by an amount equal to the volume lost by evaporation. This stage of drying is completed when the shrinking of the gel ceases. The gel stiffens as drying proceeds due to the formation of new bonds and a decrease in porosity, with the tension in the liquid rising correspondingly. The first drying stage is termed the constant rate period (CRP) due to the fact that the rate of unit evaporation per unit area of drying is independent of time [36,37].

The critical point is the point at which the shrinkage stops and cracking is most likely to occur. The shrinkage is stopped when the gel reaches sufficient strength, as a result of increased packing density, to resist further changes. For alkoxide gels the critical point coincides with the end of the CRP. At this point the second stage of drying begins. When the gel stiffens due to shrinkage, the radius of the meniscus inside the pore becomes equal to the pore radius. This results in a high capillary pressure resulting in flow of the pore liquid to the surface of the gel where evaporation takes place. The flow of liquid is driven

by the gradient in capillary stress [38,39]. This second stage of the drying process is known as the first falling rate period (FRP1).

The final stage of drying proceeds via evaporation of the liquid within the pore, and diffusion of the liquid vapour to the surface of the gel. This final stage of drying is referred to as the second falling rate period (FRP2). There are no further dimensional changes within the gel during this stage, however there is a loss of weight until equilibrium is reached, which is determined by the ambient temperature and partial pressure of water.

2.6.3 Thin films

One of the advantages of the using sol-gels is that the sol is ideal for the preparation of thin films prior to gelation. Thin sol-gel films are commonly prepared by processes such as spinning, dipping or spraying. The thin films prepared and discussed in this thesis were prepared using the spin coating technique.

Spin coating is a common method for depositing thin, uniform films onto substrates. Spin coating can be divided into four stages: deposition, spin-up, spin-off, and evaporation [40]. During the deposition stage excess sol is dispensed onto the surface of the glass slide. The spin-up stage describes the flow of the liquid outwards, driven by centrifugal forces. During the spin-off stage, excess liquid flows to the perimeter and leaves as droplets. As the film thins, there is a greater resistance to flow therefore the rate of removal of excess liquid by spin-off slows down [28]. The final stage of spin coating involves evaporation becoming the primary mechanism for film thinning.

2.6.4 Precursor Structure

The growth and gelation mechanisms are essentially the same for bulk and thin film formation, however there are several differing factors in the structural evolution of films [41]. In the case of thin films the deposition and the evaporation steps overlap. Therefore evaporation of the sol, which compacts the structure, competes with continuing condensation reactions, which stiffen the structure resulting in an increase in resistance to compaction. In bulk sol-gel formation the gelation and drying stages are separated. The aggregation, gelation, and drying steps occur on a much shorter time scale for thin films, in comparison to bulk sol-gels, and depend on the evaporation rate of the solvent (typically water and methanol). Thin film networks have considerably less crosslinking (formed during ageing) than present in bulk gels, due to the shorter duration of the deposition and drying stages. The flow of fluid due to draining, evaporation, or spin-off combined with attachment of the sol to the substrate surface results in shear stress within the film during the deposition, whereas bulk gels are not constrained in any direction [28].

2.6.5 Film Cracking

The disadvantage of sol-gel films is their tendency to crack during the drying stage. Cracking can be described as “drying failure” , and as the name suggests it describes the failure of the system during the drying stage [42]. The stress in a film is approximately equal to the tension in the liquid. Therefore, as the gel becomes more rigid the tension in the film becomes equal to the capillary stress, which results in the film shattering. Inorganic films which are thinner than approximately 0.5 microns do not tend to crack, however films which are over 1 micron thick are difficult to dry without cracking [43-45]. It is therefore important to be able to control the spin coating in order to prepare crack free thin films.

2.6.6 Sol-gel chemistry

The work presented in this thesis is based on the formation of sol-gels from alkoxide precursors. In the presence of an acid, it is likely that an alkoxide group is protonated in a rapid first step, as illustrated by the schematic shown in figure 2.9 for protonation of TMOS.

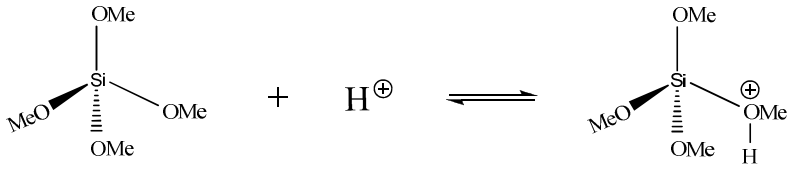

Figure 2.9. Schematic for protonation of TMOS

Electron density is withdrawn from the silicon atom, making it more electrophilic and thus more susceptible to attack from water. This results in the formation of a penta-coordinate transition state with significant SN2-type character [28]. The transition state decays by displacement of an alcohol and inversion of the silicon tetrahedron, as seen in figure 2.10.

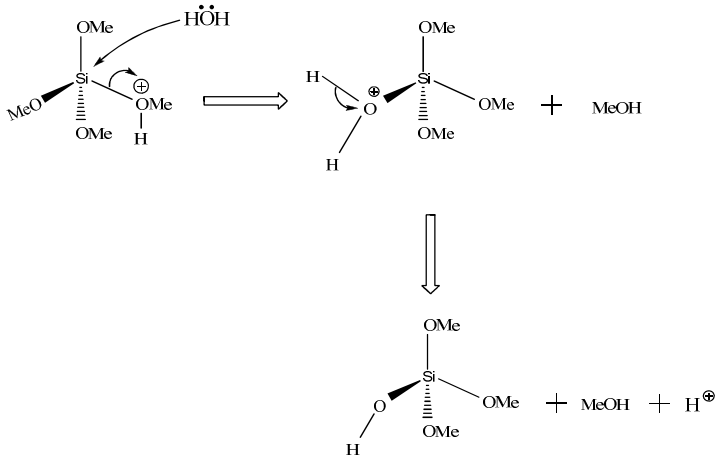

Figure 2.10. Schematic for hydrolysis of TMOS.

The reaction rate of the hydrolysis increases with the strength of the acid, therefore HCl acid is commonly used as a catalyst. The hydrolysis can also be catalysed by a base, and proceeds via a nucleophilic mechanism. However, the rate of base catalysed hydrolysis occurs at a much slower rate at the same catalyst concentration. Due to the basic nature of the alkoxide oxygen's they tend to repel the nucleophile, ^{-}OH [46].

2.6.7 Bioencapsulation in sol-gel nano-pores

The encapsulation of proteins within an inorganic silicate matrix was first reported in 1990 by Braun and co-workers [47]. Although, there have been successful attempts at the encapsulation of proteins within sol-gel materials there is still relatively little known about the local environment, such as polarity, of the entrapped proteins.

During gelation a hydrated bio-compatible silica matrix containing pores of typically ~10 nm are formed around individual protein molecules, matching their size whilst connecting to the network by smaller pores of ~1 nm; the latter acting as a conduit for analytes of interest while excluding potentially interfering macromolecules. The optical transparency afforded by silica sol gels makes them suitable for application as sensors based on fluorescence changes. These features are ready-made for sensing applications and potentially could be used to simulate natural conditions in single protein research with a view to answering such fundamental questions as - do all proteins of a given type fold by the same pathway and how do proteins aggregate?

2.7 Protein Fluorescence

The early works of Debye and Edwards [48] and many others [49,50], have shown that proteins in aqueous solution possess intrinsic fluorescence in the near-ultraviolet region (UV). Intrinsic protein fluorescence can be used for structural and physiochemical studies of proteins. The absorption and emission of proteins in the near-UV region are due to the presence of aromatic amino acid residues, namely tryptophan, tyrosine, and phenylalanine. Interpretation of the fluorescence spectra of proteins requires a knowledge of the spectroscopic properties of these amino acids in the isolated state [51,52].

Tryptophan is the most widely studied of the fluorescent aromatic amino acids, due to its high quantum yield, resonance energy transfer from phenylalanine and tyrosine to tryptophan being common in proteins, and its sensitivity to its environment which can provide information on conformational changes. Tryptophan has the highest quantum yield of the aromatic amino acids, with a quantum yield of ~0.2 in aqueous solution at room temperature [53].

Tryptophan, in aqueous solution, has two absorption bands, with absorption maxima at 280 nm (ϵ_{280} = 5600 M^{-1} cm^{-1}) and 218 nm (ϵ_{218} = 33,000 M^{-1} cm^{-1}), and peak emission centred at ~ 348 nm. The absorption bands are as a result of electron-vibrational $\pi \longrightarrow \pi^*$ transition in the indole ring [54]. Indole has absorption peaks present at 225 nm and 270 nm. The presence of the electron withdrawing carboxyl group in close proximity to the indole ring, results in the shift in absorption bands for tryptophan. The structure of indole and tryptophan are shown in figure 2.11.

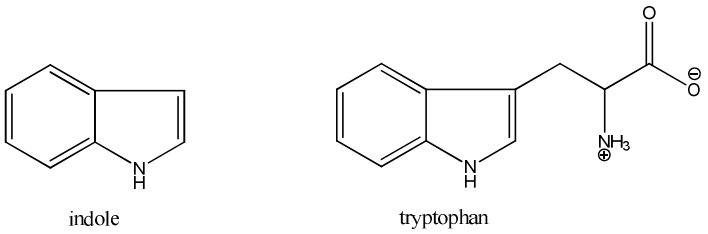

Figure 2.11. Tryptophan and indole structure (at pH 7).

Tryptophan can be selectively excited between 295-305 nm, which avoids excitation of tyrosine in proteins.

Early studies of the fluorescence lifetime measurement of tryptophan indicated that it decayed with a single exponential [55,56]. However, tryptophan studied over the pH range 2 to 10.6 indicated a three exponential decay. The three lifetimes were assigned to the cationic, zwitterionic, and anionic forms [57]. It is now largely understood that the origin of the multi-exponential decay of tryptophan is due to the presence of rotational conformational isomers (rotamers), as will be discussed in further detail in §3.3.

Tyrosine, in neutral aqueous solution, has its absorption maxima at 275 nm (ϵ_{275} = 1230 M^{-1} cm^{-1}) and 222 nm (ϵ_{222} = 8000 M^{-1} cm^{-1}), and peak emission centred at ~ 303 nm. The absorption is due to $\pi \longrightarrow \pi^*$ transitions [54]. The quantum yield of tyrosine in neutral aqueous solution is ~ 0.14 [53]. Tyrosine has a lower quantum yield than tryptophan, but it may still contribute significantly to protein fluorescence. However, the fluorescence from tyrosine can be easily quenched by nearby tryptophan residues due to resonance energy transfer. The fluorescence decay for tyrosine (pH 5.5) yields a double exponential. Again this is attributed to the rotamer model which is widely accepted for tyrosine.

Phenylalanine is weakly fluorescent in comparison with the other two aromatic amino acids, with an absorption maxima in neutral aqueous solution, at 257 nm of 200 M^{-1} cm^{-1}, and peak fluorescence emission centred at ~ 282 nm. It has a quantum yield of ~0.02 [58].

However, the availability of improved LED sources allows for the direct excitation of this residue [59]. Although weak, a further understanding of the phenylalanine residue could lead to further information on energy transfer within proteins.

The fluorescence decay of phenylalanine was until recently believed to be monoexponential. However, the there has been recent evidence that is not the case, and that it does indeed display a multiexponential decay which is dependent on pH [60]. This provides evidence for the application of the rotamer model to phenylalanine, which is not surprising considering it contains the same branched groups as both tryptophan and tyrosine, which are largely responsible for the effect described by the rotamer model. The structure of both tyrosine and phenylalanine can be seen in figure 2.12.

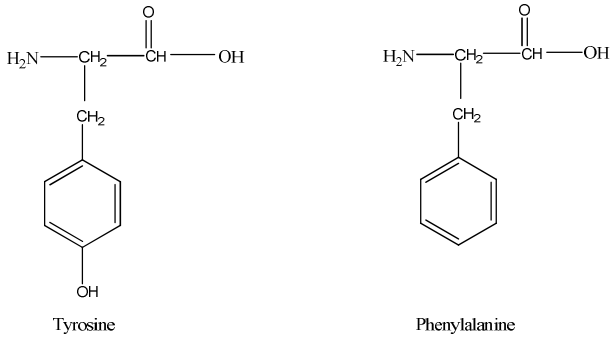

Figure 2.12. Structure of aromatic amino acids: tyrosine and phenylalanine.

3. Amino acid: Phenylalanine

3.1 Introduction

The application of light emitting diodes (LED) as excitation sources for time-domain fluorescence study is not a new area of research. The application of such sources has been well documented. However, the ability to characterise intrinsic protein fluorescence by direct excitation of aromatic amino acids, has until recently been difficult due to limitations in LED technology. The absorbance bands of the fluorescent aromatic amino acids, tyrptophan, tyrosine and phenylalanine can be excited using LED sources at 295, 280 and 265 nm respectively [59,61,62] with previous LED wavelength limitation at ~370 nm [63], which precluded most intrinsically fluorescent proteins .

Progress in the fabrication of deep ultraviolet (UV) AlGaN light emitting diodes (LED) has been considerable in recent years [64]. Recently the first results on exciting protein fluorescence using 280 nm [62] and 295 nm [61] LED sources have been demonstrated by the Photophysics Research Group at Strathclyde University in collaboration with Horiba Jobin Yvon IBH Ltd, Glasgow. The development of deep UV LED's not only makes the study of protein fluorescence simpler and less expensive than the mode-locked lasers or flashlamps used previously, but also offers the potential of new miniaturised implementations such as lab-on-a-chip technology using immunoassays, thereby opening-up new approaches to point-of-care and rapid diagnostics. In biomolecular research this technology is providing researchers with cheaper, more reliable and simpler means to achieve excitation of not only amino acids and protein, but also other important fluorophores such as nicotinamide adenine dinucleotide (NADH). Compact ultraviolet (UV) LED devices offer advantages over traditional deep-UV sources by way of ease of use, rapid collection times and less susceptibility to interferences [62].

In the following section, fluorescence lifetime measurements were performed using a 265 nm AlGaN light-emitting diode (LED) excitation source and recorded using an IBH 5000U fluorescence lifetime system (Horiba Jobin Yvon IBH Ltd., Glasgow, UK) with excitation and emission monochromators incorporating a holographic grating in a Seya-Namioka geometry.

3.2 Characteristics of 265 nm LED

The 265 nm LED operates stably with an output power of typically ~1.3 µW average and ~2.3 mW peak at 1 MHz repetition rate (Hamamatsu power meter type no. S1227-1010 BQ placed as close as possible to the LED). The output power of the 265 nm LED compares favourably with the previously reported nanosecond sources ie 280 nm LED [62], 295 nm LED [61], and hydrogen flashlamp [65] (Table 3.1).

Source	Average Power/µW	Peak Power/ mW	Pulse width/ns
IBH 5000F Flashlamp	0.45	12	0.9
265 nm light emitting diode	1.32	2.3	1.2
280 nm light emitting diode	0.70	1.2	0.6
295 nm light emitting diode	0.35	0.6	0.6

Table 3.1. Source average power, peak output power, and pulse width. IBH NanoLED drive circuitry operated at 1 MHz to produce LED pulsing and TCSPC synchronisation. Note that the flashlamp power is integrated between 200 and 900 nm.

The instrumental full width of half maximum (FWHM) of the 265 nm LED, including the detector response, is ~ 1.2 ns. This is a little broader but comparable to the flashlamp (~0.9 ns) and other UV LEDs [61,62].

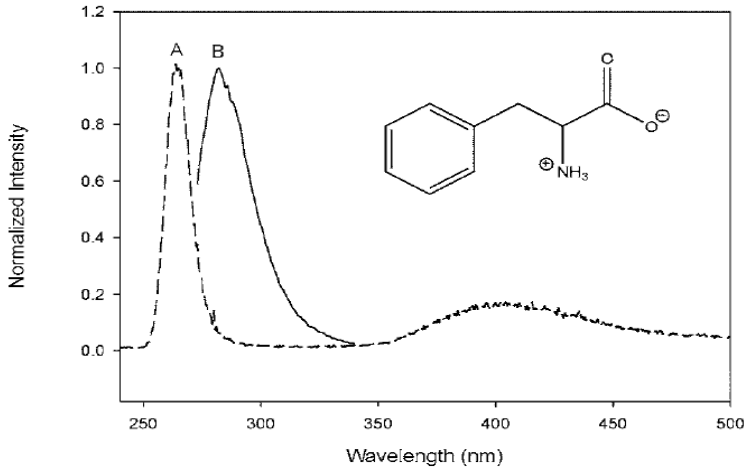

Figure 3.1. (A) Emission spectral profile of 265 nm LED with 2 nm bandwidth. The FWHM of the main peak is ~12 nm. (B) Fluorescence spectrum of 3 X 10^{-6} mol l^{-1} phenylalanine at pH of 7.4 excited using the 265 nm LED. The structure of phenylalanine is also shown.

The spectral width of the 265 nm LED, shown in figure 3.1 (A), was recorded using a SPEX FluoroMax 2 with 2 nm spectral bandwidth. The spectral FWHM observed is ~12 nm, which is consistent with values reported for other LEDs [61,62].

The spectrum also shows a weaker broadband emission at ~400 nm, a feature which was reported as being present in the spectral profile for a 280 nm LED [62]. For this reason the source output needs to be prefiltered to ensure that this longer wavelength component is not detected along with the Stokes shifted fluorescence. This long wavelength emission cannot be used for exciting other fluorophores due to its long decay time previously reported for the aforementioned 280 nm LED as being in the region of ~500 µs [62]. In a previous report by Shatalov et. al. [66] in which they described the time-resolved electroluminescence of an AlGaN-based light-emitting diodes with emission at 285 nm, they reported the presence of a long-wavelength emission band centred at 330 nm. They

concluded that the long-wavelength emission band centred at 330 nm is caused by the carrier recombination from the conduction band to the deep acceptor levels in the p-AlGaN layer at room temperature.

Hitherto the excitation of phenylalanine fluorescence decay required the use of bulky, expensive or high maintenance pulsed sources such as synchrotrons [67], mode-locked lasers [68], or flashlamps [65] and/or working at potentially problematical high concentration ($>10^{-4}$ mol l^{-1}) where self-absorption or excimers can occur. The LED enables the fluorescence decay of weakly emitting phenylalanine to be measured routinely in the condensed phase, even in dilute solution, the results of which will be discussed in this chapter.

3.3 Rotamer model

The complex multi-exponential fluorescence decay kinetics of tyrosine and tryptophan can be described in terms of conformational isomers which display distinct decay times. The photophysical properties of the aromatic amino acids depend on the status of the amino and carboxyl groups (neutral, protonated, acylated, amidated) although they are separated from the chromophore by two methylene groups [51,52]. The multi-exponential decay kinetics have been interpreted in terms of rotamers of this side chain, which can perturb according to pH, the phenyl π electrons responsible for the fluorescence. The quenching efficiency is controlled by the orientation of the quenching groups and the process is distance dependent.

The rotamer model for tryptophan was first described by Szabo and Rayner [69], based on the Gauduchon and Whal rotamer model [70], where they interpreted the emission in terms of non-interconverting ground state rotamers of the molecule in solution. The rotamer model for tyrosine and tryptophan photophysics is now widely accepted. Because

of steric effects between the side chain of tryptophan and the polypeptide backbone, all rotamers are not equally probable. Newman projections for tryptophan rotamers [71] of the indole side chain are shown in figure 3.2. The tryptophan rotamer with the greatest population and the lifetime of 3.1 ns is (A), where the quenching group nearest to the indole is the small amino group. Rotamer C is somewhat less probable, as the larger carbonyl group is the closest one to the indole. The least likely rotamer is B, with both the amino and carbonyl group close to the indole. This rotamer may have the short lifetime of 0.51 ns. The presence of different tryptophan rotamers has been independently confirmed by NMR spectroscopy. Thus the uniqueness of three-dimensional structure appears as a somewhat a relative term, at least in solution. The structure may be better described by the presence of conformers in equilibrium.

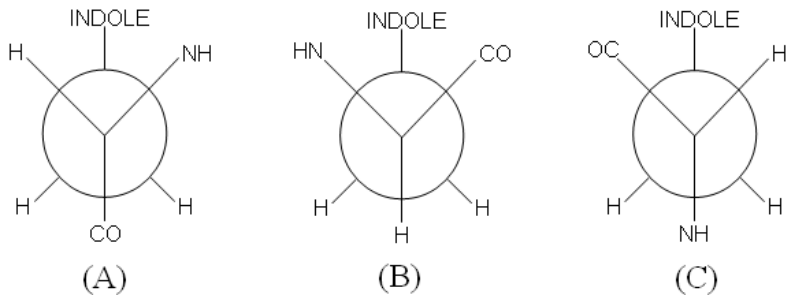

Figure. 3.2. Newman projections for tryptophan rotamers. The Newman projections indicate the rotation of the indole group about the C_{α}-C_{β} bond [71].

The presence of rotamers, however, does not fully explain the multiexponential decay in proteins containing a single tryptophan residue. As the indole ring assumes different positions in a polypeptide chain, a slightly different position of neighbouring quenching groups may also result in a multiexponential decay.

3.4 Phenylalanine

Phenylalanine with only a benzene ring and a methylene group is weakly fluorescent. The experimental sensitivity (the product of quantum yield and molar absorbtivity maximum) is especially low for this residue. Phenylalanine fluorescence is observed only in the absence of both tyrosine and tryptophan. The simple structure of phenylalanine may pre-eminently demonstrate the effect of structure on fluorescence. The presence of a hydroxyl group, as in tyrosine, causes an increase in fluorescence. If an indole ring is added as in tryptophan, the relative fluorescence intensity is increased even further. Phenylalanine is one of three fluorescent amino acids present in proteins, however its use in protein structural studies has been limited due to its low quantum yield and short wavelength of excitation.

Hitherto it has been reported that aqueous phenylalanine exhibits a mono-exponential fluorescence decay. The results presented here report a bi-exponential fluorescence decay of aqueous phenylalanine [59] observable over a wide pH range. Phenylalanine has a quantum yield of ~ 0.02, some 10× lower than that of tryptophan (Φ = ~ 0.2) [72]. Such weak fluorescence, short wavelength and energy transfer to tyrosine in proteins, has rendered phenylalanine an unpopular fluorescent probe for monitoring biological functions and protein structural studies. Despite these shortfalls however, it has been demonstrated that intrinsic phenylalanine fluorescence from calmodulin mutants can be used to gain information on calcium binding using both steady-state [73] and time-resolved fluorescence [74], and the fluorescent properties of superoxide dismutase can be obtained from intrinsic phenylalanine fluorescence [75].

There have been extensive supersonic jet studies of fluorescent amino acids cooled in the gas phase which have produced evidence for the existence of ground state conformers [76, 77-79]. In the case of L-Phenylalanine two electronic states, $\pi\pi^*$ and $n\pi^*$, are thought

to be overlapping in the S_1 state with the main transition considered to be the $\pi\pi^*$ transition [80]. The mixing between these two states would be expected to depend on the local environment and conformation of the amino and carboxylic group n-orbitals and the π^*-orbital of the carboxylic acid group with respect to the phenyl plane. Philips et. al. [79] using laser-induced fluorescence and supersonic jet cooling found spectral evidence for six conformers in tryptophan. They detected common fluorescence lifetimes among some of the conformers, and concluded that the conformer dependent lifetimes in the range 10 to 13 ns were due to interaction between the amino acid side chain group and the indole chromophore. However, the role of the inter-converting ^1L_a and ^1L_b S_1 excited states[81], known to be present in tryptophan, relative to conformers is still unclear. In the case of phenylalanine in a supersonic jet Hasimoto et. al. [78] have recently reported the presence of six conformers with a lifetime spread in the range 29 to 87 ns i.e. much greater than tryptophan. Two of these conformers were identified as intramolecular hydrogen bonded (IHB) forms, the most stable of which in the S_0 state has the shortest lifetime reported at 29ns, which is considerably shorter in comparison to the fluorescence lifetime of 68ns recorded for the other IHB conformer [78]. Whether or not the large spread in phenylalanine lifetimes can be accounted for by conformers or overlapping electronic states or a combination of both has yet to be established.

Contrastingly previous reports on aqueous phenylalanine have reported a single exponential fluorescence decay, thus suggesting a single excited conformer in the time window of the fluorescence or a number of indistinguishable conformers [68,82]. This is perhaps surprising given the multi-exponential nature of tyrosine and tryptophan fluorescence decays in solution, the multi-exponential decay observed for phenylalanine residues in transmembrane domain sequences [68] and the gas phase behaviour of phenylalanine [78].

3.5 Experimental

In the experiments described here, L-phenylalanine (>99%), volumetric standard hydrochloric acid solution, volumetric standard sodium hydroxide solution, borate buffer (pH 9.2) and spectrophotometric grade methanol (>99.9%) were obtained from Sigma-Aldrich Co. (Dorset, UK). Phosphate buffered saline (PBS) was obtained from Oxoid Ltd. (Basingstoke, UK). All fluorescence measurements were carried out on the IBH 5000U fluorescence lifetime system (Horiba Jobin Yvon IBH Ltd., Glasgow, UK) with excitation and emission monochromators incorporating a holographic grating in a Seya-Namioka geometry. The excitation and emission monochromators were tuned to 265 nm and 280 nm respectively with 6 nm bandpass. Excitation was provided by the 265 nm pulsed light-emitting diode [59] operating at 1 MHz repetition rate with a pulse width of ~1.2 ns. All samples were measured in Teflon capped 4×1×1 cm quartz type fluorometric cells (Optiglass Ltd., Essex, UK). Fluorescence decays were accumulated to 10,000 counts in the peak channel over 4,096 channels with 29 ps channel width.

Results

The fluorescence decay times and fractional intensities of aqueous phenylalanine, were measured, over a pH range of 1 to 13 and in methanol. In aqueous solution, and contrary to previous reports, a weak, but nevertheless discernible second fluorescence decay component is present at all pH values except at pH 13. The results are shown in table 3.2.

Conditions	τ_1 (ns)	f_1 (pc)	τ_2 (ns)	f_2 (pc)	$<\tau>$ (ns)	χ^2
pH 1	2.79 ± 0.07	2.0	5.94 ± 0.02	98.0	5.88	1.020
pH 4	3.81 ± 0.09	2.0	7.51 ± 0.02	98.0	7.44	1.040
pH 6	3.61 ± 0.10	4.8	7.12 ± 0.04	95.2	6.95	1.081
pH 7.4 PBS	3.48 ± 0.08	2.1	6.73 ± 0.03	97.9	6.66	1.015
pH 9.2 borate	3.84 ± 0.13	36.0	6.57 ± 0.04	64.0	5.59	1.020
pH 10	3.74 ± 0.47	2.6	7.16 ± 0.03	97.4	7.07	1.062
pH 13	4.55 ± 0.01	100	-	-	4.55	0.957
Methanol	4.90 ± 0.11	1.7	9.56 ± 0.03	98.3	9.48	0.991

Table 3.2 – Fluorescence decay components and average decay time of aqueous L-phenylalanine over a pH range of 1 to 13. Data obtained from L-phenylalanine in methanol is included for comparison.

By analogy with the other fluorescent amino acids the two component nature might be attributed to two stabilised rotamers of the side chain existing in solutions on a time scale longer than that of the fluorescence: for example (but not necessarily uniquely) L-cis-phenylalanine and L-trans-phenylalanine as shown in figure 3.3.

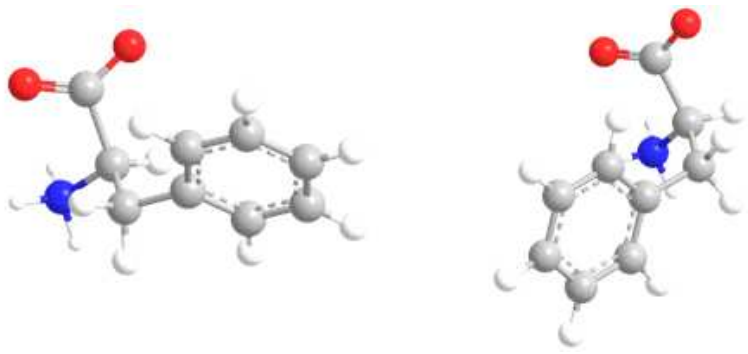

Figure. 3.3. Illustration of possible stabilized rotamers based on cis- and trans-isomers of L-phenylalanine looking along the C_α-C_α bond. Models generated from the MNDO semi empirical Hamiltonian in the MOPAC 2000 quantum mechanics package.

In the pH range 4 to 10, the two distinct decay components are one low amplitude component around 4 ns and the other high amplitude component around 7 ns. A faster

fluorescence decay in solution as compared to the super-cooled gas phase is to be expected due to increased collisional quenching in the former. It is also perhaps not too surprising to find some evidence in solution of the conformer behaviour found in the super-cooled gas phase. At pH 1, it is concluded the shorter decay times are as a result of the full protonation of the molecule as the pH is lower than the pKa of the hydroxyl group. Here, the positive charge will draw electron density away from the aromatic ring system, resulting in a quenching effect. At pH 13, the molecule will be fully deprotonated creating an environment where evidently either only one rotamer is stable or the two rotamers are indistinguishable in terms of the fluorescence decay due to the extreme negative charge, paralleling the gas phase where different conformers can give a similar decay [78,79]. Unusual behaviour is observed in pH 9.2 borate buffer solution with the increase in relative amplitude of the shorter decay component. The fluorescence decay of phenylalanine at 265 nm excitation and 280 nm emission (6 nm bandpass throughout) in pH of 9.2 buffer and fitted functions for one and two exponential components are illustrated in figure 3.4.

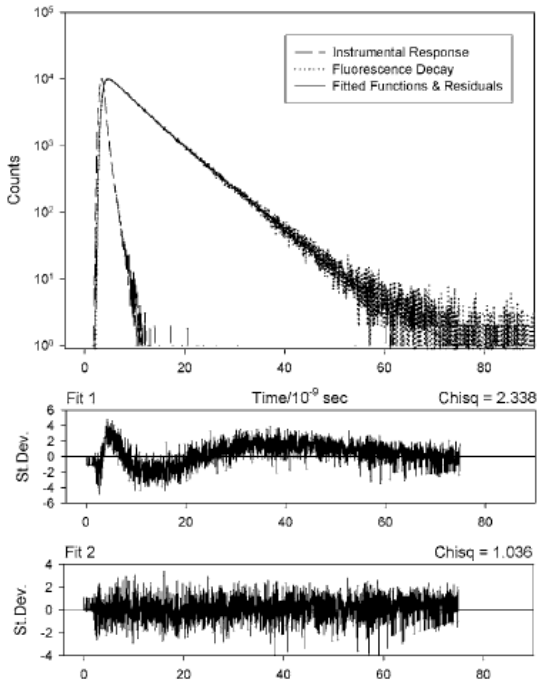

Figure 3.4. LED instrumental pulse, fluorescence decay of $3x10^{-6}$ mol l^{-1} phenylalanine in borate buffer (pH 9.2), fitted function, and weighted residuals for a bi-exponential (Fit 2) and a mono-exponential (Fit 1) model. Chi-squared values are shown for comparison.

It is clear from the chi-squared value that one decay component is insufficient to describe the kinetics and a two-component model is required. Initially, it was assumed that this was a pH effect, although as this behaviour is not observed at higher pH, it may be due to the salinity of the buffer solution, containing sodium tetraborate and borate acid, having an effect through stabilisation of both rotamers. It has been reported for indole derivatives, that the presence of different salts has a variety of effects depending on the derivative studied [83-86]. In some cases the quantum yields increased slightly while in others slight decreases were observed. The experiment was repeated many times to ensure that the results were correct and not an experimental anomaly. It should be noted that the choice of buffer is crucial when working in the UV region. In this work potassium hydrogen phthalate buffer solution (Fisher Scientific, pH 4) was initially chosen as a buffer. However the presence of an aromatic ring in the structure, shown in figure 3.4, resulted in background fluorescence making it difficult to obtain results for phenylalanine in this solution.

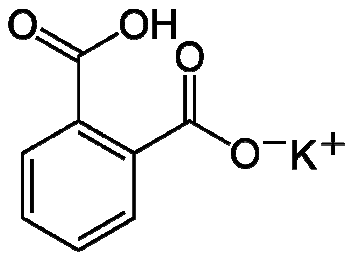

Figure 3.5. Potassium hydrogen phthalate structure.

Data obtained from L-phenylalanine dissolved in methanol replicates the bi-exponential and rotamer behaviour in a non-aqueous solvent.

3.7 Summary

While the results presented here are consistent with the existence of rotamers in phenylalanine in solution it is possible that there maybe other explanations. While influence of overlapping ππ* and nπ* states on the fluorescence decay, is not discounted, the coupling would be expected to be strong in solution, in itself favouring mono-exponential behaviour. By contrast the case for discrete fluorescence decay components associated with stabilised rotamers in fluorescent amino acids continues to be demonstrated, most recently in a maximum entropy study of the influence of quercetin on tryptophan in protein [2]. While not expecting the phenylalanine chromophore in proteins to behave identical to the results reported here, there is more similarity between the two environments than between gas and solution phase from which we are still able to draw useful comparisons.

The rotamer model for tyrosine and tryptophan photophysics is now widely accepted, but the existence of rotamers in phenylalanine has hitherto lacked supporting evidence because of its apparent mono-exponential decay in solution [50,61,67]. The findings described in this chapter differ from these previous results and suggest there is much more commonality between the photophysics of all three fluorescent aromatic amino acids than has perhaps hitherto been appreciated.

The recent availability of UV light emitting diodes allows us to probe the intrinsic fluorescence from aromatic amino acids, leading to direct measurement of protein conformation changes. With the continuing development of light sources and surface plasmon enhancement techniques, the ability to study single proteins through their intrinsic aromatic acid residues is not unrealistic. The ability to apply naturally occurring fluorescence in proteins eliminates any intrusion by dye labelling, as the current single

protein strategies utilise. Therefore the ability to understand the photophysics of these aromatic amino acids leads to a better understanding of intrinsic protein fluorescence with the hope of being able to utilise this natural tool to detect metabolites at the single molecule level, with implications to the detection and control of many diseases.

4. Silica sol-gel optimisation for bioencapsulation

4.1 Introduction

Organic fluorophores form a diverse group of probes responsive to the conditions of their local environment. As a result these fluorophores can be applied to the study of a wide-range of phenomena such as protein dynamics, calcium sensing, DNA sequencing, and membrane structures [13,87,88]. Many fluorophores have been designed (or found to have) sensitivity to parameters such as pH, polarity, hydrophobicity, viscosity, temperature, and pressure [89-93]. These parameters can occur on a macroscopic scale (i.e. solvent properties) or a microscopic scale (e.g. inside proteins and membranes).

4.1.1 Solvatochromic effect

Several dynamic processes may be involved in the Stokes' shift (§2.1), including energy loss due to dissipation of vibrational energy, redistribution of electrons in the surrounding solvent molecules induced by the changed (usually increased) dipole moment of the excited fluorophore, and specific interactions between the fluorophore and solvent or solutes including hydrogen bonding and formation of charge-transfer complexes. A precise interpretation of the solvent sensitivity of fluorophores requires a detailed knowledge of the effects of solvents on the energy levels in both the ground and excited states of the individual fluorophores. A complete quantitative description of all these processes and their effects on fluorophores is not readily available, but we can use simple theories about solvent-fluorophore interactions to interpret these spectral shifts in terms of the average environment surrounding the fluorophore.

The fluorescence emission can be further shifted to lower energy wavelengths still due to solvent effects. A bathochromic shift, describes a shift of the spectral band to lower frequencies (longer wavelengths), informally referred to as a red shift, with increasing solvent polarity. It is also called positive solvatochromism. Bathochromic shifts are sometimes accompanied by a decrease in the quantum yield of the fluorophore

6-propionyl-2-(N,N-dimethylamino)naphthalene (PRODAN), structure shown in figure 4.1, was first introduced by Weber and Farris in 1979 [94], and since this time has found widespread use as an environment sensitive fluorescent probe. PRODAN has been utilised in the study of protein binding domains [95], to probe inclusion complexation with monomeric [96] and polymeric cyclodextrins [97], the effects of high pressure on PRODAN-liquid interactions [98], the structure of lipid bilayers and cellular membranes, solvation dynamics in neat polar liquids [99], ionic liquids [100] and supercritical fluids [101,102].

The attachment to the aromatic ring system of two groups, which are respectively a good electron donor and a good electron acceptor, results in strong polarity sensitive effects. This effect is strongest when the distance between the donor and acceptor groups is at a maximum. In a naphthalene derivative this criteria is fulfilled when the groups are attached to the 2 and 6 position of the rings.

The dipole moment of PRODAN after excitation, increases as charge is transferred from the electron donating alkylamine group (NR_2) to the electron accepting carbonyl group (C=O) (intramolecular charge transfer, ICT). Rapidly, the solvent molecules reorganise around the dipole, lowering the system energy. Upon transfer of the fluorophore from water to a less polar environment there is a marked blue shift in the emission maximum

wavelength, and an increase in the quantum yield of the PRODAN, as shown in figure 4.1.

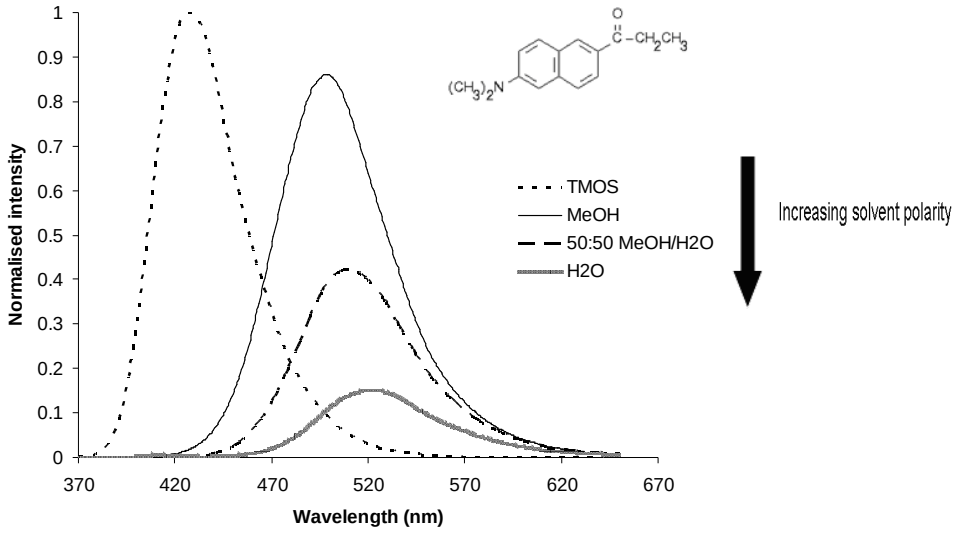

Figure 4.1. 6-propionyl-2-(N,N-dimethylamino)naphthalene (PRODAN) fluorescence emission spectra change with increasing solvent polarity. PRODAN was used at a concentration of 2.2 µM and λex - 350 nm.

4.2 Sol-gels

Porous silica sol-gels were synthesised by acid-catalysed hydrolysis of tetramethyl orthosilicate (TMOS) where methanol (MeOH) is formed as a side product.

Schematically the reaction can be written:

$$Si(OCH_3)_4 + 4\ H_2O \rightarrow Si(OH)_4 + 4\ CH_3OH \quad \text{(Hydrolysis catalysed by acid)} \qquad (4.1)$$

$$nSi(OH)_4 \rightarrow \text{porous network of } (SiO_2)n + H_2O \quad \text{(Condensation)}$$

An intrinsic problem with the preparation of silica sol-gels, using orthosilicate precursors, is the release of alcohol during the reaction process, which denatures protein through an

alteration of the native structure [103,104]. Therefore it is imperative that alcohol is removed from the sol and the internal pore solvent is pH adjusted, to within protein survival range, by the addition of phosphate and borate buffers.

4.3 Experimental

The stoichiometric equation shows that the full hydrolysis of 1 mol TMOS requires 4 mol of H_2O. In this work small volumes of sol-gels are prepared from 4.5 ml of the TMOS precursor. Molar calculations conclude that 2.2 ml of H_2O is required for complete hydrolysis at the selected volume of TMOS. In this chapter two sol-gel samples are prepared at different composition and the results compared. One sample was prepared at the stoichiometric ratio of H_2O (2.2 ml) and the second sample prepared with excess water (5 ml H_2O).

TMOS sol–gels were prepared by sonicating together, for 30 min, 4.5 ml TMOS, distilled water (one sol was prepared at stoichiomteric water volume of 2.2 ml, and a second sol prepared with excess water volume of 5 ml), and 0.1 ml hydrochloric acid (0.1 N). The sol prepared with excess water (5 ml) giving a molar ratio H_2O/TMOS = 9.4 where the excess water ensures complete hydrolysis of the orthosilicate. The sols were kept at 4 °C for 5 days, allowing the hydrolysis step to effectively reach completion without promoting gelling through the condensation steps, and only then vacuum distilled at 50 °C for ~3–5 min at 200 mbar to remove MeOH. It is essential that MeOH is removed prior to the introduction of proteins to the sol as it is harmful to biologically active molecules.

The protein pH survival range is between pH 6-8. It is therefore imperative that the sol be neutralised prior to the addition of the protein. This is achieved by the addition of phosphate buffer solution (PBS, pH 7.4) and borate buffer solution (pH 9.2), at a 50 %

v/v. Neutralisation of the sol by PBS only results in a very rapid gelation time of approximately 5 minutes. However, the addition of borate buffer solution extends the gelation time to approximately 10 minutes. This allows for the processing of the sol into monoliths and thin films. The final solution of the gel is within the protein pH survival range as determined by universal indicator.

PBS buffer solution was prepared by dissolving 1 PBS tablet (Oxoid Ltd.) in 100ml of distilled H_2O. The borate buffer solution was prepared by dissolving 1 borate tablet (Fisher scientific Ltd.) in 100ml distilled H_2O. Buffer solutions were stored at 5°C.

Steady-state fluorescence analysis was performed using a Perkin-Elmer LS 50B spectrometer with excitation at 360 nm. Steady state error was calculated using a Rhodamine 6G (R6G) reference sample. The standard deviation (S.D.) of the reference sample was calculated, with experimental errors taken as ± 1 x S.D. All fluorescence analysis was carried out using special optical glass cuvettes (Starna scientific Ltd).

4.4 Results

Calibration curves were constructed for PRODAN peak wavelength and intensity change with increasing methanol concentration in aqueous solution, until the cuvette contained only MeOH (24.68 mol L^{-1}). A linear regression plot can be seen for PRODAN peak wavelength with increasing MeOH concentration. The calibration curve for PRODAN intensity, also plotted against increasing MeOH concentration, yielded a polynomial fit. Calibration curves are shown in figure 4.2.

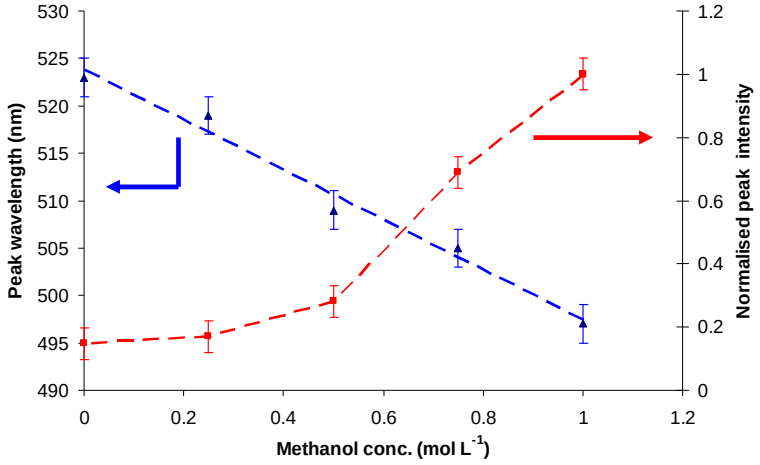

Figure 4.2 Calibration curves for PRODAN in aqueous solution with increasing concentration of MeOH. The changes in peak wavelength (-------) and normalised peak intensity (-------) are shown.

As the MeOH concentration increases there is an increase in PRODAN fluorescence intensity (shown in figure 4.2). This result is consistent with PRODAN photophysics.

Two silica sol solutions were prepared by acid-catalysed hydrolysis of TMOS, as discussed in detail in preceding sol-gel section. Both samples were prepared with identical TMOS concentration, and differing concentrations of H_2O. PRODAN fluorescence was monitored in both samples.

The PRODAN fluorescence for the sol-gel sample, prepared with a stoichiometric concentration of H_2O (molar ratioTMOS:H_2O = 4), was monitored over a five day ageing period.

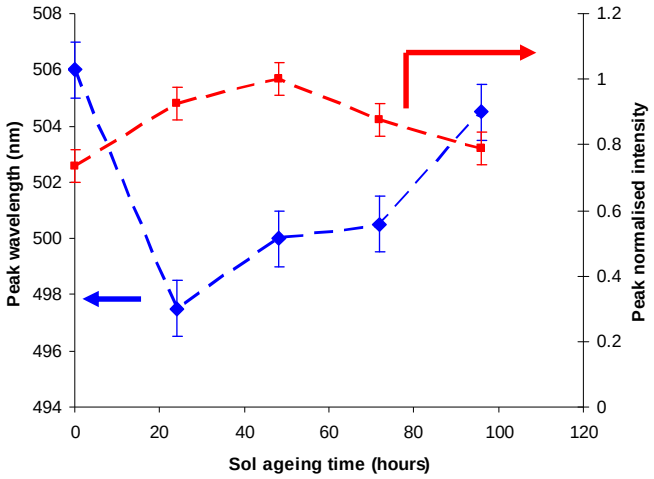

Figure 4.3. Steady state fluorescence for sol-gel prepared with stoichiometric ratio of TMOS:H_2O. The changes in peak wavelength (-------) and normalised peak intensity (-------) are shown.

The steady-state fluorescence showed a blue shift in PRODAN peak wavelength and an increase in quantum yield after 24 hours ageing, as shown in figure 4.3. The blue shift in peak fluorescence wavelength is consistent with PRODAN fluorescence in a less polar environment. The results suggest that the hydrolysis of the TMOS precursor occurs over the first 24 hours of sol ageing. As a result of this sample being prepared at a stoichiometric ratio of TMOS:H_2O, the hydrolysis step results in reaction of all water and the generation of MeOH. The change in peak wavelength of PRODAN from 506 nm to 498 nm is consistent with peak emission recorded in MeOH.

After the initial 24 hour period a red-shift in PRODAN peak wavelength was recorded, which can possibly be attributed to the electron absorption and emission transitions of PRODAN being sensitive to the solvent acidity. The presence of basic sites (the carbonyl group, tertiary amine group) can undergo significant changes with electron transition. Therefore, the electron transition in PRODAN can markedly depend on the acidic nature of the solvent [105]. The formation of silicic acid, as a result of TMOS hydrolysis, initially results in a sol of acidic pH. Silicic acid, however, is inherently unstable and

rapidly condenses with itself with the elimination of water forming, dimers, trimers, and eventually resulting in the formation of a gel. The polymerisation of silicic acid monomers results in an increase in the pH of the sol.

This change in PRODAN fluorescence corresponds to a change in the polarity of the probes local environment. The blue-shift in peak wavelength and increase in fluorescence intensity over the first 24 hours provides a good indication that the hydrolysis occurs over this period.

The sample prepared with a higher concentration of H_2O (excess, molar ratio H_2O/TMOS = 9.4) showed no significant change in PRODAN peak wavelength, however, there was a significant increase in quantum yield after a 24 hour ageing period, as shown in figure 4.4. This result is consistent with PRODAN fluorescence in a lower polarity environment, which again is attributed to the formation of MeOH during the TMOS sol-gel hydrolysis step. The change in PRODAN fluorescence occurs again over the first 24 hours which is consistent with results for the sol-gel prepared at a stoichiometric ratio of TMOS:H_2O.

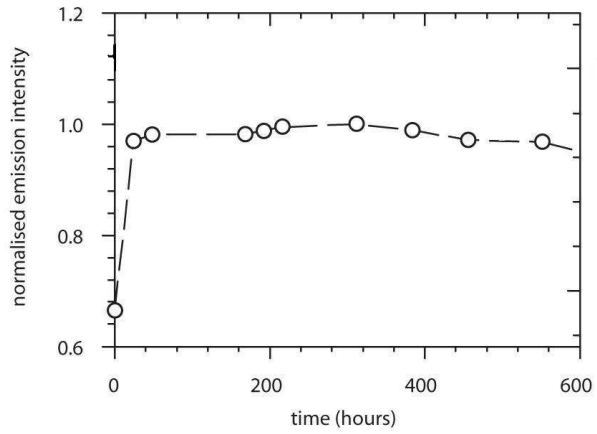

Figure 4.4. Normalised PRODAN fluorescence intensity for TMOS sol-gel prepared with excess H_2O as measured over time.

The increase in peak fluorescence intensity indicates that hydrolysis is occurring over the initial 24 hour ageing period. Therefore, to be able to monitor hydrolysis kinetics and thus pinpoint the ageing time required for the hydrolysis a second sample of the same composition was monitored on an hourly basis. The results are shown in figure 4.5.

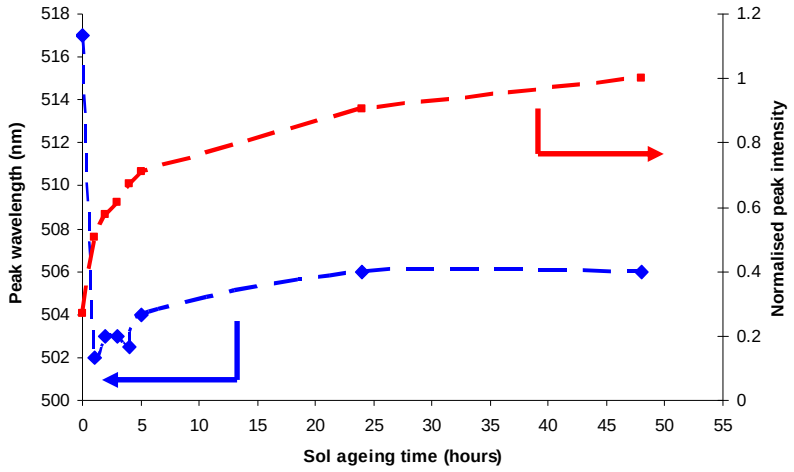

Figure 4.5. Normalised PRODAN fluorescence intensity in aTMOS sol-gel prepared with excess H_2O as measured over sol ageing time. The changes in peak wavelength (-------) and normalised peak intensity (-------) are shown.

There is an initial decrease in peak wavelength over the initial 1 hour period. This suggests that the hydrolysis reaction initiates at a fast rate. The peak wavelength stabilizes after this initial period. However, the fluorescence intensity increases for a 48 hour period after the initial measurement. This suggests that the hydrolysis is still continuing over the first 48 hours of the gel ageing.

A further experiment was performed to ensure that the change in PRODAN fluorescence was in fact reporting on the hydrolysis step. Two aqueous samples were prepared containing TMOS, at concentrations present in the sol, and MeOH at concentration calculated by assuming complete hydrolysis of TMOS (ie 4x conc. 1:4 molar ratio of TMOS:MeOH). The fluorescence intensity of PRODAN in the MeOH sample was of a

higher magnitude with respect to the sample containing TMOS, with no significant change in PRODAN peak wavelength between both samples. TMOS having less polar character (and thus PRODAN having higher quantum yield) than MeOH, it would be expected that the highest peak fluorescence intensity would be measured in the TMOS sample. However, the highest peak intensity was recorded on the MeOH sample. The higher concentration of the latter (4x), results in higher fluorescence intensity with respect to the PRODAN fluorescence intensity in the TMOS sample. This result is in agreement with the trend seen for sol ageing over first 24 hours, for the sol sample prepared at higher water concentration, where there is a change in fluorescence intensity without a change in peak wavelength. Over the first 24 hours there is unreacted TMOS, which becomes hydrolysed with the resultant formation of MeOH.

The result also provides further evidence that the change in PRODAN fluorescence is a direct result of MeOH formed during TMOS hydrolysis as shown in figure 4.6.

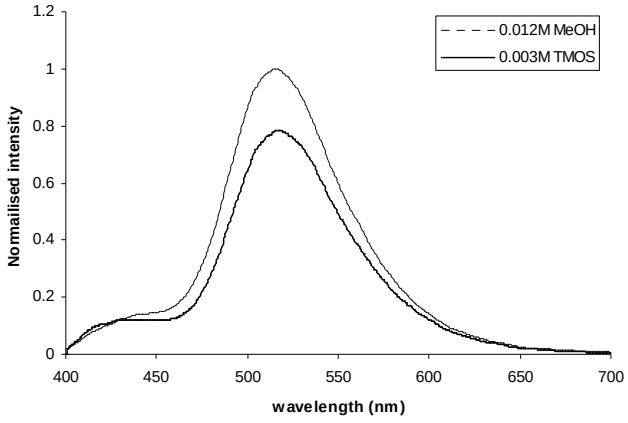

Figure 4.6. PRODAN steady-state fluorescence in aqueous solution containing MeOH and TMOS. The peak λ for both samples was 521 nm.

The change in PRODAN fluorescence was measured on a set of samples with differing vacuum distillation time. Increase in rotary evaporation time results in red shifted PRODAN fluorescence associated with more polar environment. After 180 seconds rotary evaporation time, the PRODAN peak emission wavelength is consistent with that found in an aqueous environment, as shown in figure 4.7. A decrease in PRODAN peak fluorescence intensity is observed, which is associated with an increase in environment polarity. As methanol is removed, PRODAN responds to a more water like polar environment as can be seen by a decrease in intensity as shown in figure 4.7.

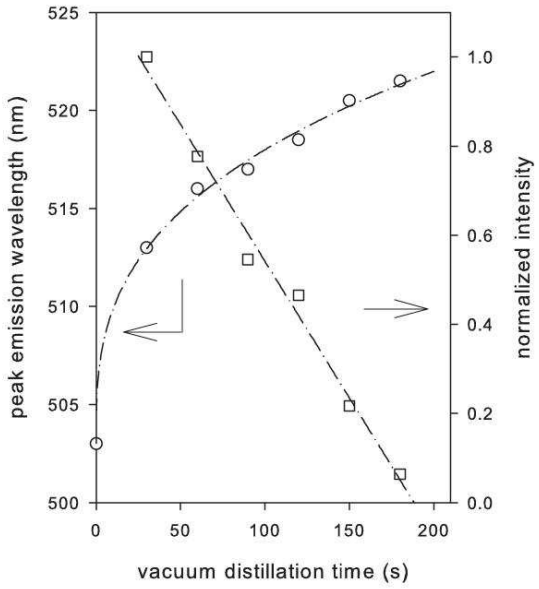

Figure 4.7. PRODAN steady-state fluorescence as a function of increasing vacuum distillation time.

After vacuum distillation, phosphate buffer solution and borate buffer solution were added to the remaining sol volume, 15ml of each respectively. Change in the sol pH rapidly increases the gelation time (t_g) resulting in the formation of a gelled monolith in the cuvette. The addition of buffers neutralizes the sol-gel and provides a suitable internal pore liquid for protein encapsulation within the sol-gel pores. Therefore the fluorescence

response of PRODAN was measured in phosphate buffer solution, borate buffer solution and a combination of both buffers as per the sol-gel neutralisation protocol, and normalised with respect to PRODAN fluorescence in distilled H_2O. As can be seen from the spectra, shown in figure 4.8, PRODAN peak wavelength corresponds to an aqueous environment in each of the buffer solutions. There is also no significant change in peak intensity for any of the buffer solutions with respect to PRODAN peak intensity in distilled H_2O.

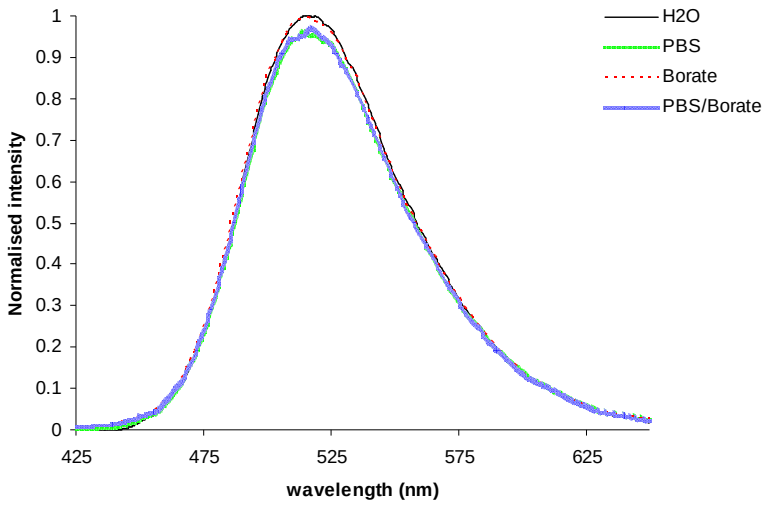

Figure 4.8. Steady-state spectra for PRODAN in various buffer solutions.

The fluorescence spectra of PRODAN in a sol was measured, prior to rotary evaporation and also prior to the addition of phosphate and borate buffer solutions, and the results compared with those for a sol prepared with removal of methanol and neutralisation. The alcohol free and neutralised sol was then measured again at 1 hour after the gel point. The PRODAN spectra recorded in the sol prior to vacuum distillation, shows blue-shifted peak wavelength and higher fluorescence intensity, in comparison with PRODAN in an aqueous environment. The PRODAN spectra of the sol after vacuum distillation and addition of buffers shows a red-shifted fluorescence peak and decrease in quantum yield compared with the spectra recorded prior to removal of methanol and pH adjustment.

The peak wavelength and quantum yield are consistent with PRODAN fluorescence corresponding to an aqueous environment. The spectra recorded 1 hour after the gel point showed little significant difference from spectra recorded prior to gel point. The results are shown in figure 4.9.

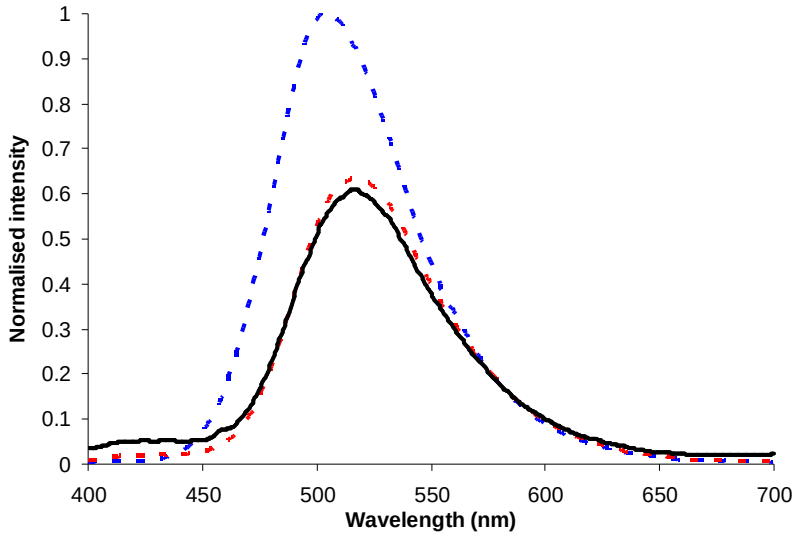

Figure 4.9. PRODAN fluorescence spectra recorded in TMOS sol-gels, prior to the removal of methanol by vacuum distillation (--------), and after, methanol has been removed (--------). For comparison the PRODAN spectra in the methanol free gel 1 hour after the gel point is shown (——).

4.5 Sol-gel encapsulated hexokinase.

The biocompatibility of the optimised sol-gel method was ascertained by the entrapment of the enzyme hexokinase, which is important in the metabolism of glucose.

The intrinsic fluorescence of hexokinase in solution (excitation = 295 nm, emission = 330 nm) is attributed to tryptophan residues in the protein. Each monomer subunit of hexokinase consists of two lobes with a cleft in the middle; binding of glucose to the active site in the cleft causes the two lobes to move closer together, and with this a

quenching of fluorescence occurs [106]. Therefore an improved technique for the encapsulation of hexokinase could lead to the development of a glucose sensor based on a change in intrinsic protein fluorescence.

Hexokinase was encapsulated in two sol-gels prepared using different methods. Gel A was prepared at a stoichiometric ratio of TMOS:H_2O, and after 5 day ageing period, the sol was vacuum distilled for two minutes. Gel B was prepared with excess H_2O and aged for five days, and the resulting sol vacuum distilled for 3 minutes. The results were compared with hexokinase in H_2O. Hexokinase was used at a concentration of 10^{-6} mol L^{-1}, and excited at 290 nm. The results are shown in figure 4.10.

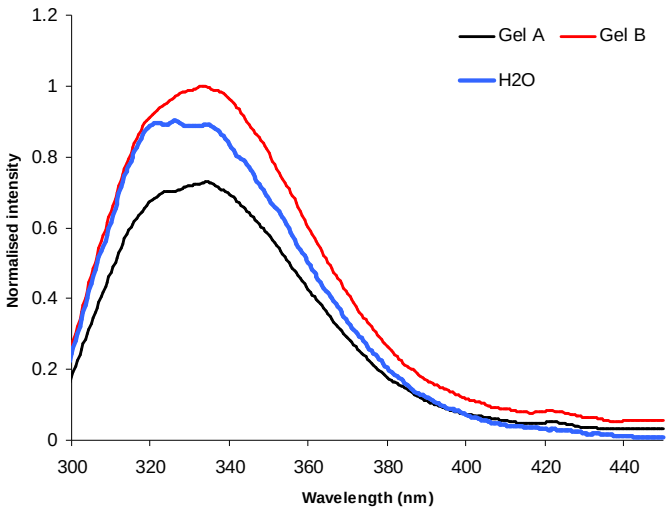

Figure 4.10. TMOS sol-gel encapsulated hexokinase and in H_2O. Hexokinase was used at a concentration of 10^{-6} mol L^{-1} and λex - 290 nm.

The results illustrate the improvement offered by the PRODAN optimised method (gel B). The peak fluorescence intensity shows a marked increase in the optimised method (28%) as compared with Gel (A). The intrinsic fluorescence of hexokinase in gel A is

quenched, by possibly insufficient removal of alcohol or unreacted TMOS. The optimisation of the vacuum distillation technique by PRODAN fluorescence ensures that any detectable alcohol has been removed. Also, the presence of excess H_2O ensures the complete hydrolysis of TMOS.

The optimised method shows an increase in hexokinase peak fluorescence intensity compared with hexokinase sample in H_2O. This effect is possibly as a result of slower oxygen diffusion through the porous sol-gel network. Tryptophan residues in proteins are known to be dynamically quenched by oxygen [107,108]. The quenching effect of oxygen on fluorescence, and the protection offered by sol-gels and application to single molecule fluorescence will be discussed in a later chapter.

4.6 Summary

The ability of PRODAN to report on the polarity of its local environment, provided an ideal choice with which to monitor the hydrolysis step for the formation of a TMOS sol-gel, and also report directly on the internal environment of the sol-gel nano-pores. The sensitivity of the probe provided a good indication for the completion of the hydrolysis stage and complete removal of methanol, by vacuum distillation, through change in sol polarity. The removal of methanol is essential for protein survival and thus the application of PRODAN as an indicator for its removal provides an efficient method for ensuring that no detectable methanol remains in the sol prior to the introduction of protein.

Timings for pre-aging and distillation of the silica sol were determined by investigating a parallel series of samples containing the environmentally sensitive fluorophore 6-propionyl-2-(N,Ndimethylamino) naphthalene (PRODAN) to report on the progression of

the hydrolysis reaction and on the composition of the distillate. With increasing MeOH concentration the response of PRODAN fluorescence is twofold, first a shift can be observed in the peak wavelength, as compared to water (in H_2O the spectrum peaked at 521 nm and in MeOH at 498 nm) and second an increase in fluorescence intensity, i.e. quantum yield. The increase in peak wavelength and decrease in quantum yield shows the sensitivity of PRODAN to the removal of methanol, and provided a vacuum distillation time for complete removal of detectable methanol. The sensitivity of PRODAN to its environment provided a method of measuring the time required for the completion of the hydrolysis and distillation steps. This ensured that the pore liquid was free of methanol such that protein could be added without denaturation.

The improved ability of this method to the measurement of intrinsic fluorescence is demonstrated by the increased fluorescence intensity of hexokinase immobilised in sol-gel nano-pores. With the application of this method, and the continuing development of ultra-violet light sources and understanding of intrinsic amino acid fluorescence, it may be possible in the future to monitor single proteins without the requirement of attaching bulky fluorescent tags as previously required. And furthermore, the specific ability to encapsulate hexokinase may have application to single-molecule glucose sensing as a function of intrinsic fluorescence change.

The PRODAN optimised protocol, described in this chapter, provides a generic approach for the encapsulation of sensitive proteins. Furthermore, the method can be applied to the immobilisation of proteins for single-molecule fluorescence study.

The method we have described here has allowed for the encapsulation of the environment sensitive trimeric form of Allophycocyanin (APC), in both monolith form for ensemble measurement and in thin films for single-molecule confocal measurement, as discussed in further detail in the §5.4 and §6.4.2 respectively

5. Allophycocyanin

5.1 Introduction

APC belongs to the phycobiliprotein family which are present as aggregates in phycobilisomes that lie near chlorophyll reaction centres in Cyanobacteria and Rhodophyta (blue–green and red algae respectively) [109]. Each allophycocyanin monomer contains two phycocyanobilin chromophores, shown in figure 5.1, which are labelled as α84 and β84 to denote its position in the protein backbone.

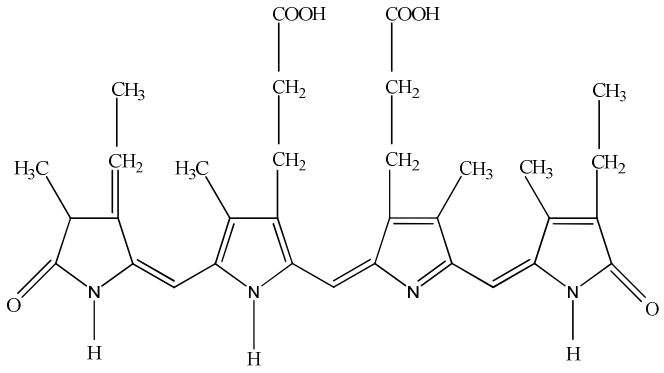

Figure 5.1. Phycocyanobilin Chromophore

The monomer has a fluorescence peak emission at 638nm. Naturally, the close proximity of the monomers results in dipole interaction resulting in exciton splitting as illustrated in figure 5.2. The chromophores are considered to have excitation energy delocalised between them, with an associated red–shifted fluorescence peak emission at 660nm. The trimeric state of allophycocyanin is thus very sensitive to environment, with changes resulting in dissociation to monomeric form.

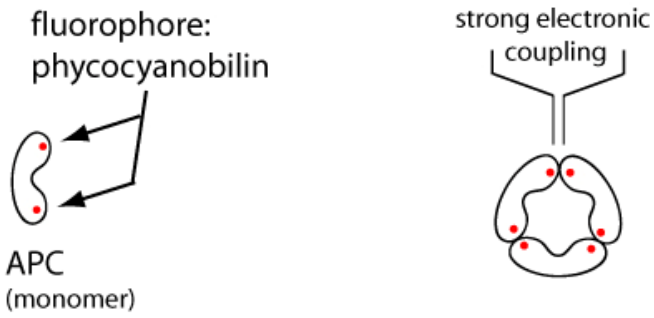

Figure 5.2. Schematic for monomeric and trimeric form of allophycocyanin

The trimeric APC structure in aqueous buffer solution has a fluorescence emission peak at 660 nm associated with exciton splitting of the chromophore and until the present work has required the use of cross-linking to preserve the trimeric form down to the single-molecule level [110,111].

Previous attempts at preserving the trimeric structure of APC in a sol-gel matrix have been unsuccessful, even when maintaining neutral pH either before or after gelation [112], presumably due to the protein's extreme sensitivity (through such mechanisms as disrupted hydrogen bonding) to the vicinal solvents and pH changes generated, resulting in dissociation to the monomeric form [113].

5.2 Sol-gel preparation

TMOS sol–gel was prepared by sonicating together, for 30 min, 4.5 ml TMOS, 5 ml distilled water and 0.1 ml hydrochloric acid (0.1 N); giving a molar ratio H_2O/ TMOS = 9.4 where the excess water ensures complete hydrolysis of the orthosilicate. The APC was not added at this point (as commonly done), but the sol pre-aged by typically storing it for five days (i.e. much longer than previous protocols [114] at +4°C, allowing the hydrolysis step

to effectively reach completion without promoting gelling through the condensation steps, and only then vacuum distilled at 50ºC for circa 5 min at 300 mbar to remove MeOH. Finally, the sol was neutralised by the addition of a mixture of 15ml PBS (phosphate buffer saline, pH 7.4) and 15 ml borate buffer (pH 9.2). This both neutralises the sol and dilutes any remaining polymerisation products.

The removal of MeOH and pH adjustment of the sol induces a rapid transition to the gel state. Therefore APC had to be added quickly to the sol at this point in order to achieve a homogenous dispersion of the protein. The optimum times for sol ageing and vacuum distillation of MeOH, for this encapsulation protocol were obtained using PRODAN [94] in parallel measurements on equivalent sols used for protein encapsulation as described in §4.4.

5.3 Experimental

APC (Sigma-Aldrich Ltd) was used without further purification. Stock solution was prepared in PBS (pH 7.4, Oxoid Ltd, Basingstoke, UK). Sol-gels were prepared by the sonication of 4.5 ml TMOS, 5 ml H_2O, and 0.1 ml HCL (volumetric standard 0.1010M) for 30 minutes at 50°C. The sols were aged for 5 days under refrigerated conditions prior to vacuum distillation and neutralisation of the sol. The stock solution of APC was diluted into the sol to give a final concentration of 1.28×10^{-7} mol dm^{-3}. The sol was then left to reach the gel point in the optical glass cuvette.

Ensemble fluorescence measurements were recorded on a Jobin-Yvon Fluoromax 2 spectrometer.

5.4 Results and discussion

For up to 500 hours the fluorescence emission peak of encapsulated APC was close to 660 nm demonstrating dominance of the aqueous trimeric form, but with a gradual decrease, until rapidly decreasing to 638 nm as shown in figure 5.3. During this period the gel loses weight and we associate these changes with pore shrinkage and greater exposure to silanol groups as aqueous buffer evaporates and the gel dries, a process which could be ameliorated by re-hydration. After 500 hours the fluorescence emission peak shifted rapidly to 638 nm, corresponding to the monomer [113].

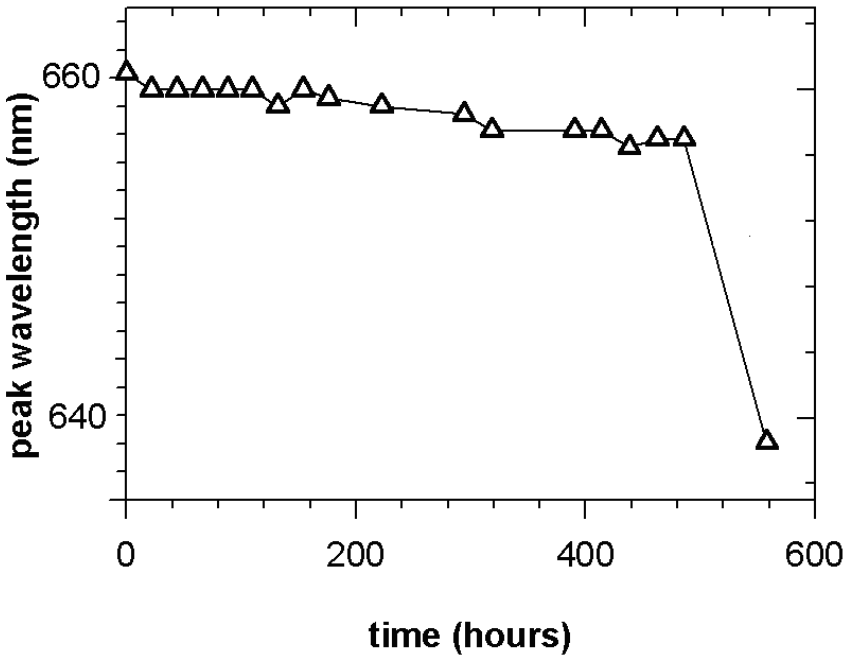

Figure 5.3. Fluorescence peak wavelength (Δ) of APC encapsulated in a sol-gel nano-pore measured over 560 hour period.

The APC trimer fluorescence spectrum encapsulated using the pre-aged method described here as compared with a sol-gel we prepared without pre-aging by the method described by Ferrer et. al [114], is shown in figure 5.4. The latter resulted in dissociation of the trimer as shown by the blue shift in the peak wavelength, and an increase in full width

half maximum (FWHM). A monomer fluorescence spectrum, prepared in aqueous solution at pH 4, is also shown for comparison.

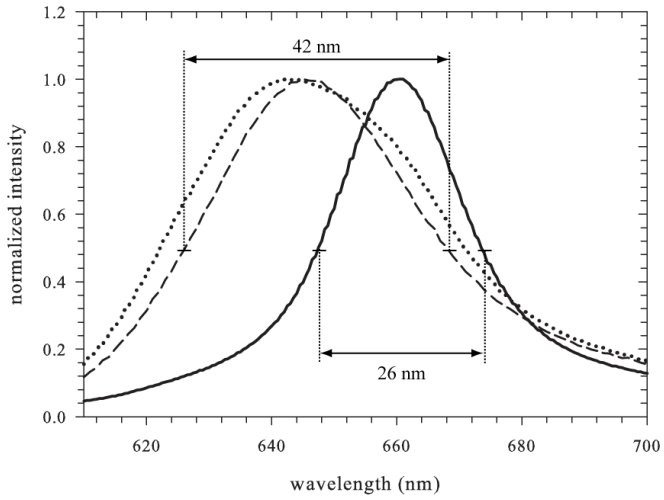

Figure 5.4. Fluorescence spectra of APC (excitation at 550 nm) encapsulated in a sol-gel monolith prepared according to the new protocol with pre-aging (——) and according to previous protocols [114] without pre-aging (– – – –). FWHM are indicated. For comparison the emission spectra of APC in its monomer form (·····) is also shown (recorded for APC dissolved in water at pH 4).

5.4.1 Fluorescence lifetimes

The fluorescence lifetime of decay component τ_1 for the monomeric form, prepared by the addition of methanol to APC/PBS solution, shows an increase in both fluorescence lifetime and relative amplitude with respect to the trimeric form in PBS, as shown in table 5.1. The change in fluorescence lifetime and relative amplitude is likely to be as a direct result of dissociation of the trimer and thus cessation of exciton splitting between the α and β chromophores.

The fluorescence lifetimes, and relative amplitudes, recorded for APC encapsulated in a sol-gel nano-pore after 24 hours is directly comparable to the results for APC in its

trimeric form in buffer solution. The trimeric form is the dominating form present after this gel ageing period as confirmed by steady-state fluorescence spectra peak emission.

After sol-gel ageing for 720 hours there is an increase in the fluorescence lifetime (τ_1), and also an increase in relative amplitude (f_1). The results are consistent with the fluorescence lifetime (τ_1) and relative amplitude (f_1) recorded for the monomeric form, prepared by the addition of methanol to APC/PBS solution.

APC sample	τ_1 (ns)	f_1 (%)	τ_2 (ns)	f_2 (%)	χ^2
Trimeric form (APC PBS)	0.156 ±0.060	1.710	1.760 ±0.010	98.290	0.970
Monomeric form (APC PBS/MeOH)	0.725 ±0.090	14.980	1.940±0.020	85.020	1.240
APC sol-gel (24 hours)	0.116 ±0.020	3.310	1.730 ±0.010	96.690	0.970
APC sol-gel (720 hours)	0.717 ±0.060	18.530	1.730 ±0.010	81.470	1.070

Table 5.1. Fluorescence lifetimes for APC in trimeric and monomeric form in solution and encapsulated in TMOS sol-gel nano-pores.

Despite the additional difficulties of observation, the sol-gel matrix permits detection of trimeric APC down to 2 x 10^{-11} mol dm^{-3}, as shown in figure 5.5. This compares to sensitivities of APC in PBS recently reported of 2 x 10^{-12} mol dm^{-3} trimer using fluorescence at 660 nm and 1 x 10^{-13} mol dm^{-3} using surface enhanced resonance Raman scattering (SERRS) [115] (the latter without distinguishing between the monomer and trimer). SERRS and fluorescence analysis was carried out on a Renishaw Microscope 1000 with a Renishaw RL633 632.8 nm helium-neon laser and 50 X, 0.5 numerical aperture long-working distance

objective. The accumulation time was 10 s and the resolution 2 cm^{-1}. Measurements were carried out in 250 µl microtitre plates.

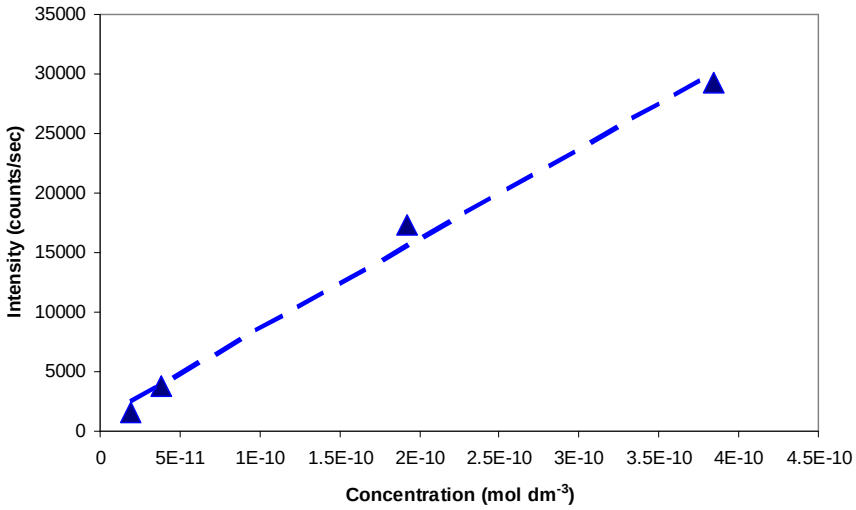

Figure 5.5. Trimeric APC detection limit in TMOS sol-gel monolith measured with Renishaw microscope 1000 (λex 632.8nm)

5.5 Summary

APC dispersed in silica sol-gels prepared according to the protocol presented in this report remains in a trimeric form for up to 500 hours before dissociating. This is evident from the fluorescence emission spectra where a band can be seen centred at 660 nm corresponding to the exciton coupling of phycocyanin chromophores localised in different subunits of APC. At this time the solvent is also expelled from the silica monolith and accumulates to a ~1 mm thick liquid layer on the top of the sample, and thus the change in protein aggregation state is possibly related to pore shrinkage and increased exposure to silanol groups.

To illustrate the importance of silica sol pre-aging on the stability of APC, the results of encapsulation in the method described in this thesis was compared with the previous state of the art preparation method reported by Ferrer et al [114] . The emission spectra recorded on APC dissolved in a sample without pre-aging (latter method) is consistent with the monomeric form, i.e. a blue shift in the peak wavelength and an increase in full width half maximum as compared to the spectra recorded on APC in the trimeric form with the encapsulation method described here.

Fluorescence lifetimes were recorded for trimeric and monomeric forms in buffered solution. The lifetimes recorded for the trimeric form were in agreement with fluorescence lifetimes recorded for the APC encapsulated in a sol-gel for a 24 hour period. The fluorescence lifetime for a sol-gel sample which was aged for 720 hours was in agreement with the sample recorded for the monomeric form in solution.

It was previously reported that phycocyanin fluorescence can be detected from freely diffusing APC molecules in PBS buffer solution at a concentration of 2×10^{-12} mol dm^{-3} [115]. Here the detection limit, for ensemble measurement, in a silica sol-gel has been demonstrated as 2×10^{-11} mol dm^{-3} despite the additional difficulties of observation such as light scattering.

6

6. Single-molecule fluorescence

6.1 Introduction

The capability for single molecule detection (SMD), which has been fully realised only in the last decade or so, has yet to be exploited in clinical medicine. Amongst the reasons for developing SMD methods in medicine is the assay of analytes present at ultra-low concentrations in the early stages of disease (e.g. tumour markers for early diagnosis of cancer or cytokines for the prediction of cardiovascular disease and type 2 diabetes) or in established disease (e.g. suppressed thyroid stimulating hormone in thyrotoxicosis). Time-related intermediates, such as those occuring during enzyme-catalysed reactions also could be identified. Most importantly, macromolecules, which have subtle conformational differences, can be detected and counted. Instead of the measurement of ensembles, where averaging renders minor forms undetectable, SMD may allow the pathology to be related, for the first time, to the pattern distribution of single molecular species. The prion disorders and other protein-folding diseases (e.g. Creutzfeld-Jacob disease) are obvious examples where sensitive early diagnosis is currently impossible and where structure-specific SMD has a high chance of clinical value. Fluorescence lends itself to SMD of biomolecules because of extreme sensitivity (single-photon), its non-invasive and non-destructive nature, and its multidimensional specificity, which enables identification of species in a mixture such as cell cytosol. Fluorescence wavelength, intensity, excited state lifetime, spatial location and polarisation can all depend on molecular structure. Fluorescence spectroscopy and microscopy are established techniques for studying molecular ensembles, but conventional fluorescence microscopes have a diffraction limited spatial resolution of ~ $\lambda/2$, typically 300 nm. Amongst the technologies for SMD by fluorescence microscopy

(wide field, confocal, total-internal reflection) scanning near field optical microscopy (SNOM) has by far the best resolution at $\lambda/10 \sim 50$ nm. This is achieved by a metal-coated, narrow fibre optic tip (emitting evanescent waves) held ~ 5-10 nm away from the sample in the so-called near field as opposed to the far field used by conventional microscopes. The limited area thus excited in SNOM enables selection of just one molecule and dramatically reduces both background fluorescence and scattered light (Rayleigh and Raman), which might otherwise contaminate the detection of individual fluorescence photons from single molecules.

However, despite the resolution advantages offered by SNOM, it has been shown that far-field confocal microscopy can be experimentally more convenient [116,117]. The single molecule images in this chapter were taken using confocal microscopy.

6.2 Single-molecule fluorescence

Single molecule detection has been demonstrated by single molecule imaging [118-120] , lifetime measurement of the excited states of single molecules [116,120,121], and single molecule spectroscopy [122,123].

In a fluorescence image, a spot will be considered as emission from a single molecule if it fulfils the following criteria. (i) The size of the spot must be of the same order as the diffraction-limited size of the illumination focus in the confocal set-up or must be considerably smaller in the near field. (ii) The signal intensity must be of the order of that expected considering the properties of the molecule, the intensity of the illumination, and the efficiency of the optical detection path. (iii)The density of spots per area must relate to the concentration of dye molecules in solution. (iv) The bleaching process should occur in

a single event with a discrete intensity drop to the background level and should not present intermediate intensity values [124].

Rhodamine 6G (R6G) dye molecules are a good choice for single molecule imaging due to there high quantum efficiency (Φ_f = 0.95) and photostability (photobleaching quantum yield $\Phi_p = 5.7 \times 10^{-7}$). The single molecule fluorescence of R6G molecules is well documented [118, 125-127] and therefore provided a good choice of fluorophore to initially try and image single molecules using the confocal microscope.

Fluorescence blinking describes the disappearance of fluorescence intensity from a single molecule, and is as a result of transition of the molecule to a non-fluorescent triplet state (T). Fluorescence blinking is a characteristic of single-molecules and therefore provides direct evidence for the detection of single-molecules. During single molecule imaging, as measured using confocal microscopy, some of the molecules disappear on subsequent scanning, as shown by single rhodamine 6G (R6G) image in figure 6.1. This is because the single molecules are blinking and/or photobleaching during the observation.

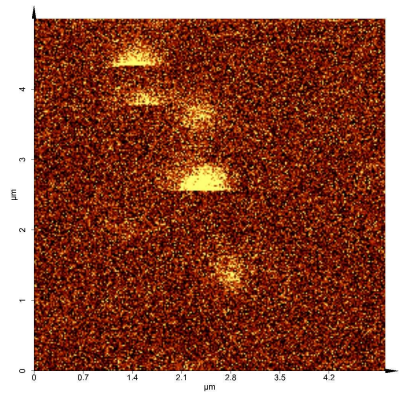

Figure 6.1. Fluorescence blinking for R6G

Blinking occurs when molecules undergo intersystem crossing to the triplet state. These molecules remain dark until they return to the ground state [10], and once again get promoted to an excited singlet state. In some cycles they are bleached, as illustrated by the Jablonski diagram shown in figure 6.2.

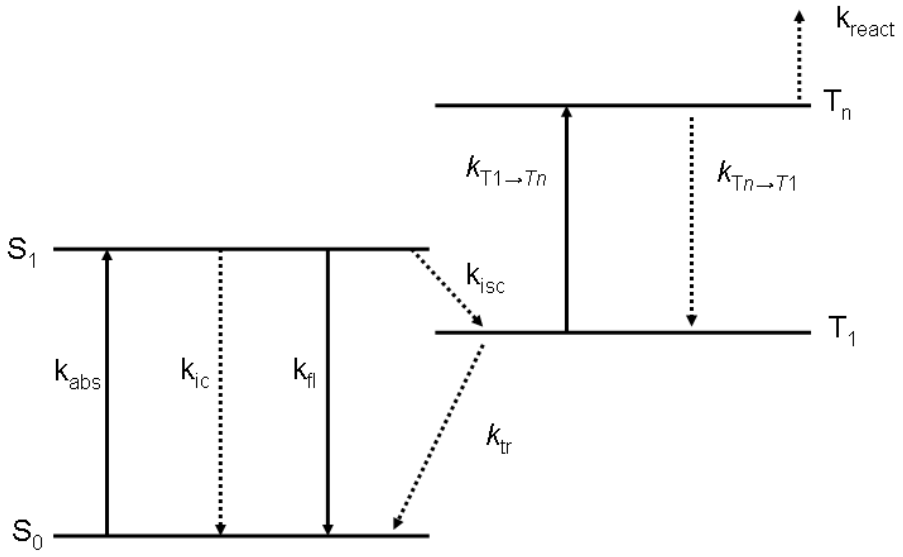

Figure 6.2. Jablonski diagram of the relevant states for photobleaching

Absorption (k_{abs}) from S_0 to S_1 may lead to nonradiative internal conversion (k_{ic}), fluorescence (k_{fl}), or intersystem crossing (k_{isc}) to T_1. From T_1, the molecule may relax back to S_0 (k_{tr}), or absorb a second photon ($k_{T1\rightarrow Tn}$) and go to T_n. From there, the molecule may either relax back to T_1 ($k_{Tn\rightarrow T1}$) or react (k_{react}), leading to irreversible photobleaching.

Collisions with paramagnetic molecular oxygen send molecules more readily into a triplet state after excitation. Photobleaching, as a result of reaction with oxygen whilst in the triplet state, poses a fundamental limitation to the information content of single molecule fluorescence measurement [128]. Ideally, a single fluorophore should last long (slow

photobleaching) and not show temporal fluctuations of fluorescence intensity as a result of transition to a triplet state.

The spin coating of the fluorophore in polymer thin films should offer some protection from photobleaching. However, to observe single fluorophores for extended periods of time, a method to remove O_2 from solution is required, as will be discussed in a later chapter.

6.3 Experimental

Thin films for single-molecule confocal fluorescence microscopy were prepared by spin coating 30μL of R6G (Fluka) stock solution prepared in poly(methylmethacrylate) (PMMA, Sigma-Aldrich, Mw ~ 350,000) on a washed glass microslide cover slip. R6G was prepared to a concentration of 10^{-10} M in PMMA, and the PMMA stock solution was prepared to a concentration of 5mg/ml in chloroform (Sigma-Aldrich).

Thin sol-gel films, for single molecule measurement were formed by diluting the APC stock solution into the alcohol free neutralized sol and spin coating to form the film. The concentrations of the protein for single molecule measurement were typically 10^{-10} mol l^{-1}.

Microscopy measurements were performed using an *a*-SNOM (WITec GmbH) aligned for confocal microscopy in reflection mode. Excitation with an Nd:YAG laser (532 nm) was delivered by a single-mode optical fibre. The beam was collimated and focused using an infinity corrected microscope objective to a diffraction-limited spot. Fluorescence was collected by the same objective and focused to a multi-mode fibre coupled to a single-photon avalanche photodiode (APD). The sample was placed on a piezoelectrically driven

scanning stage. A 2D image was acquired by scanning the sample line by line and plotting signal from the APD. Single molecule spectra were recorded using a CCD/Spectrograph (Andor Model DV401A-BV/ Princeton instruments Model SP2300i), interfaced to the *a*-SNOM through an optical fibre. The microscope can be seen in figure 6.3.

Figure 6.3(A) Schematic for single molecule confocal microscopy experimental set up. (B) Hard at work searching for elusive single molecules on *α*-SNOM (WITec GmbH).

6.4 Results: Single R6G fluorescence

Typical blinking, of an R6G molecule, can be observed in figure 6.4, where the intensity drops to the background level and the molecule stays dark over time periods of typically milliseconds to seconds. The intensity difference, of individual molecules, is thought to be as a result of different orientations of the fluorophore relative to the polarisation of the incident light.

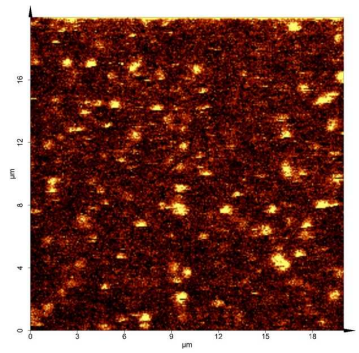

Figure 6.4. Confocal fluorescence image showing fluorescence emission from single Rhodamine 6G molecules in a PMMA thin film. The concentration of R6G was 10^{-10} mol L^{-1}.

6.4.1 Single molecule detection: Filter effect

In order to detect single molecules it is essential to eliminate scattered light. The correct combination of filters is crucial to cut down the background noise, in order to observe single-molecule fluorescence. The importance of the filters is illustrated in figures 6.5 and 6.6.

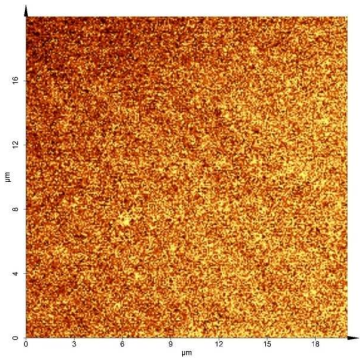

Figure 6.5 shows a confocal image of R6G in a PMMA thin film. R6G was used at a concentration of 10^{-10}M. The image was recorded by scanning over a 20x20 μm area and a 550 nm long pass filter (LP) was used eliminate background noise signals.

The confocal image (figure 6.5) shows no evidence of single molecule fluorescence. The fluorescence signal is lost in the high level of background noise. However, when a second

570 nm LP filter is added, the single molecule R6G fluorescence can be observed (evidenced by blinking), as shown in figure 6.6. The longer wavelength filter (relative to the typical peak wavelength of R6G) is required for single molecule detection.

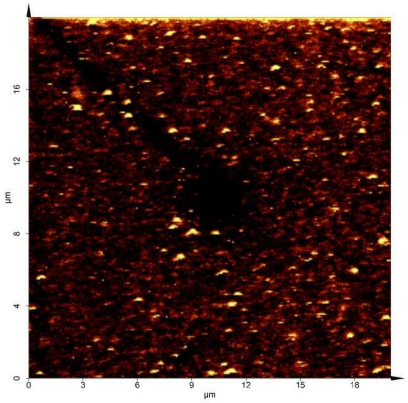

Figure 6.6 shows the confocal image over the same 20x20 µm shown in figure 6.5. This scan was recorded using a combination of both a 550 and a 570 nm LP filters.

This experiment illustrates the importance of correct filters, in order to improve signal to noise ratio for single-molecule fluorescence detection.

6.4.2 Allophycocyanin Single molecule Fluorescence

Typical single molecule fluorescence images of APC molecules encapsulated in silica sol-gel, as evidenced by blinking, are shown in figure 6.7. Sol prepared as previously described and containing APC at low concentration (typically $\leq 10^{-9}$ mol dm^{-3}) was applied onto a microscope slide. Images obtained by focusing on the gelled sample surface using bright light illumination with a Nikon 100x objective were acquired at a depth of circa 1 µm beneath the surface. Fluorescence images were collected using a 645 nm long-pass filter.

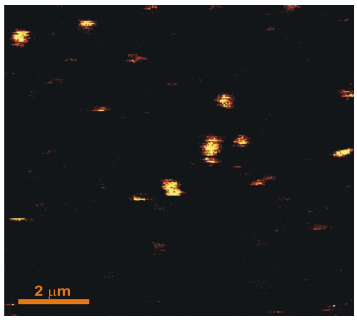

Figure 6.7. Single molecule APC fluorescence in sol-gel nano-pores.

The single molecule images display a range of sizes and shapes as the fluorophore is sometimes bleached during a sample scan. Figure 6.8 shows the corresponding single-molecule emission spectra to be consistent with APC in the trimeric form. For comparison the emission spectrum recorded on a single APC molecule under the same conditions but without the removal of methanol and pH adjustment. In the latter case APC is clearly shown to be dissociated into the monomeric form, illustrating the importance of the sol-gel optimisation on protein survival.

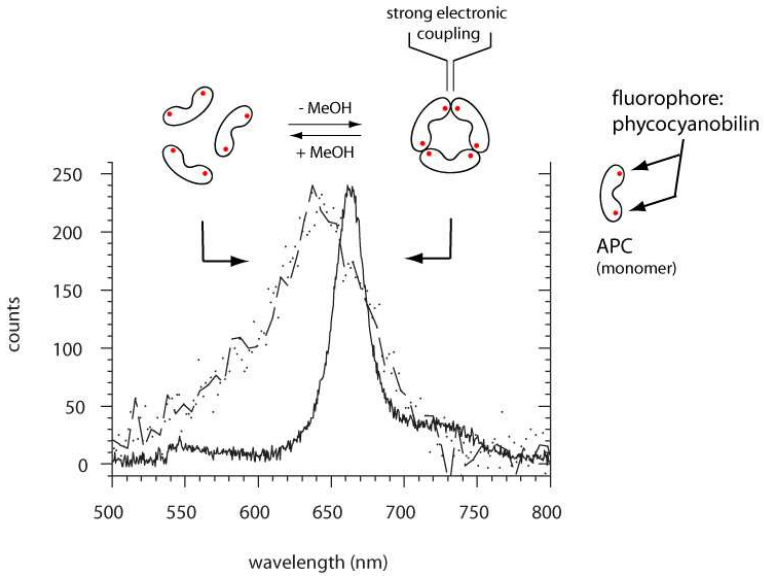

Figure 6.8. Trimer (——), and monomer (– – – –), fluorescence spectra for single APC molecules entrapped in the pores of a sol-gel thin film. The spectra have been normalised to equal intensity (counts/sec) and the baseline set to zero.

Due to the close proximity of the APC monomer emission spectra to the excitation source wavelength, a 550 nm notch filter was required to eliminate the laser source. It can be seen from figure 6.8 that any signal recorded at blue shifted wavelengths from 550 nm is due to random noise.

6.5 Summary

Single molecule detection is a difficult technique and represents the ultimate level of sensitivity. The signal to noise ratio needs to be as efficient as possible. R6G has a high quantum efficiency and relative photostability, and was therefore chosen as a fluorophore, in this work, for the initial detection of single molecules. Initially the problem with the detection of R6G single molecules was the choice of filters. The correct choice of filters, are important to improve the signal to noise ratio for single molecule detection.

Fluorescence blinking provides direct evidence for singe molecule detection. During this state the molecules “switch off” as they intersystem cross to a triplet state. The images shown in this chapter for R6G show this effect and therefore provide evidence for single molecule detection. The application of this fluorophore for single molecule detection allowed for understanding and improving of the confocal technique for recording single molecules, prior to the imaging of less quantum efficient and photostable fluorophores and proteins.

The ability to entrap a single protein molecule and control its aggregation, as demonstrated with APC, illustrates the potential of single molecule fluorescence for studying the bio-molecular interactions that underpin diseases such as the fatal prion disorders of protein folding (BSE, Creutzfeld-Jacob disease and possibly Alzheimer's and Parkinson's diseases)

at their most fundamental level, with potentially step-change implications for generic understanding of disease pathology and therapeutics. Additionally, encapsulating APC in silica sol-gel nano-pores is a further step towards metabolic sensing e.g. glucose assays using APC labelling of the glucose-binding lectin, concanavalin A [129]. Also, this technology may provide the basis for integration within “lab-on-a-chip” sensors which are capable of bringing to bear the whole panoply of fluorescence techniques and technology. This includes for example, intrinsic protein fluorescence excited with ultra-violet light emitting diodes [43,46,47], microfluidics [130], fluorescence resonance energy transfer to detect metal ions either directly [131] or indirectly using a chelate [132] and anisotropy [133].

7. Oxygen scavenging

7.1 Introduction

Organic fluorophores are prone to irreversible photobleaching due to photochemical reactions mainly photo-oxidation, which limits the number of photons emitted. Although the effect is not always influential during ensemble measurement, it is always paramount in the collection of data at the single-molecule level where oxygen efficiently reduces the fluorescence lifetime by promoting other quenching mechanisms, e.g. inter-system crossing to a "black" triplet state. The quantum yield for photobleaching varies between fluorophores, with typical values ranging between 10^{-5} – 10^{-7} [134,135]. The inverse of the photobleaching quantum yield effectively determines the total number of emitted photons on average before photobleaching [136].

Quenching of the fluorophore excited state occurs when the excitation energy is transferred to the oxygen molecule, generating the first excited state of the oxygen molecule, which is known as the singlet oxygen ($^1O_2$). There is a resultant decrease in fluorescence intensity and the occurrence of photobleaching. The latter occurs due to self-sensitisation through reaction of the fluorophore, in the ground singlet state, with the highly reactive $^1O_2$ species [137]. The quantum yield for photobleaching varies greatly among fluorophores [138].

Singlet oxygen also reacts with amino acids such as cysteine, histidine, tryptophan, tyrosine, phenylalanine, as well as guanosine in deoxyribonucleic acid (DNA) [139]. As well as having an effect on intrinsic fluorescence of aromatic amino acid, oxidative damage impairs the folding and function of biomolecules.

Although some medical applications take advantage of photo-sensitisation (photodynamic therapy), it is generally accepted as being a negative effect. Many fields such as development of solar concentrators [140], solid-state lasers [141], and single molecule spectroscopy [142,143] and detection suffer from photosensitisation, and therefore there is a lot of current research being currently done to improve the stability of dyes.

The photo-survival of fluorophores can be extended by minimising the presence of triplet-state oxygen and its highly reactive metabolites, such as singlet oxygen ($^1O_2$), hydroxyl radical (OH) and hydrogen peroxide H_2O_2. This can be achieved through deoxygenation [144], the addition of oxygen scavengers such as ascorbic acid, propyl gallate, and the glucose oxidase/catalase (GODCAT) system, flooding the sample with inert gas such as argon or nitrogen [145], or operating in a vacuum [146].

7.1.1 Ascorbic acid

Ascorbate acts as an antioxidant by being available for energetically favourable oxidation.

Reactive oxygen species oxidise (take electrons from) ascorbate to form dehydroascorbate through the free radical intermediate monodehydroascorbate, as illustrated in the schematic diagram shown in figure 7.1. The reactive oxygen species are reduced to water while the oxidised forms of ascorbate are relatively stable and unreactive.

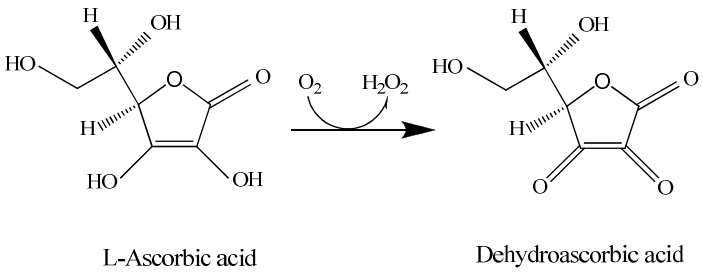

Figure 7.1. Schematic for the reaction of L-Ascorbic acid with oxygen

The retardation of photobleaching can be achieved by the addition of ascorbic acid, through the quenching of radical oxygen species [147,148,149].

7.1.2 Solubility of Oxygen

The concentration of oxygen in water at room temperature (~25^{o}C) and 1 bar pressure is 1mM. In air with a normal composition the oxygen partial pressure is 0.2 bar.

Solubility, amount of gas dissolved in a liquid, is related to pressure by Henry's law:

$$C = K_H P \qquad (7.1)$$

Where C is the concentration of dissolved gas, K_H is Henry's constant for gas in a particular solvent (K_H= 1 x 10^{-3} mol/L.atm for oxygen in H_2O), and P is the partial pressure of the gas above the solution.

Gas solubility is always limited by the equilibrium between the gas and a saturated solution of the gas. Therefore, concentration of dissolved Oxygen in a sample, in air at room temp, is ~ 0.2 mM.

7.1.3 Oxygen diffusion

In the case of collisional quenching, the quencher must diffuse to the fluorophore during the lifetime of the excited state. At room temperature an oxygen molecule has a diffusion coefficient of ~ 2.5 x 10^{-5} cm^2 s^{-1}

The root-mean-square distance $\sqrt{\Delta x^2}$ that a quencher can diffuse during the lifetime of the excited state (τ) is given:

$$\sqrt{\Delta x^2} = \sqrt{2D\tau} \qquad (7.2)$$

Where D is the diffusion coefficient.

In the following section the effectiveness of ascorbic acid as a method for removing oxygen from solution will be investigated.

7.2 Experimental

Spectrophotometric grade methanol (MeOH, 99+%, Sigma-Aldrich) was sonicated for 15 minutes at 50°C, in order to deoxygenate the solvent. Ascorbic acid (Sigma-Aldrich, Dorset) was dissolved in the deoxygenated MeOH to give a stock solution of 1 x 10^{-3} mol l^{-1}. The stock solution was diluted to give the final desired concentration.

All fluorescence lifetime measurements were carried out on the IBH 5000U fluorescence lifetime system (Horiba Jobin Yvon IBH Ltd., Glasgow, UK). The excitation and emission monochromators were set to 340 nm and 370 nm respectively with 6 nm bandpass. Excitation was provided by the 340 nm pulsed light-emitting diode operating at 1 MHz repetition rate with a pulse width of ~1.0 ns.

7.3 Results

The fluorophore 1-Pyrene Sulphonic acid (1-PSA), as shown in figure 7.2, was selected as a probe for oxygen due to its relatively long excited state lifetime (~ 50 ns). Pyrene and

its derivative have previously been used to probe for the presence and concentration of quenchers such as potassium iodide, acrylamide, and oxygen [150].

From equation 7.2, it can be calculated that in the lifetime of 1-PSA an oxygen molecule can diffuse a distance of ~165 Angstroms. Therefore, there is a high probability of interaction of the fluorophore with oxygen.

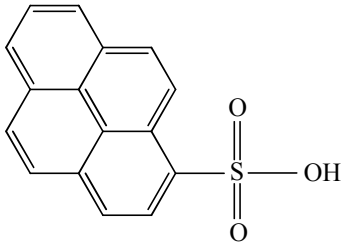

Figure 7.2. 1-PSA structure.

The steady state results for the addition of ascorbic acid to an aqueous solution containing the probe 1-PSA can be seen in figure 7.3. The normalised integrated intensity is plotted against increasing concentration of ascorbic acid.

Initially there is an increase in fluorescence intensity of 1-PSA with increasing ascorbic acid concentration. However, the fluorescence intensity finally reaches a plateau. The results suggest that the addition of ascorbic acid removes oxygen from solution and results in an increase in fluorescence intensity, however, since ascorbic acid reacts with oxygen at a 1:1 stoichiometric ratio it is clear from the results that the complete removal of oxygen is not achieved, since the concentration of dissolved oxygen in solution as calculated from Henry's law is ~ 0.2 mM. Results are shown in figure 7.3.

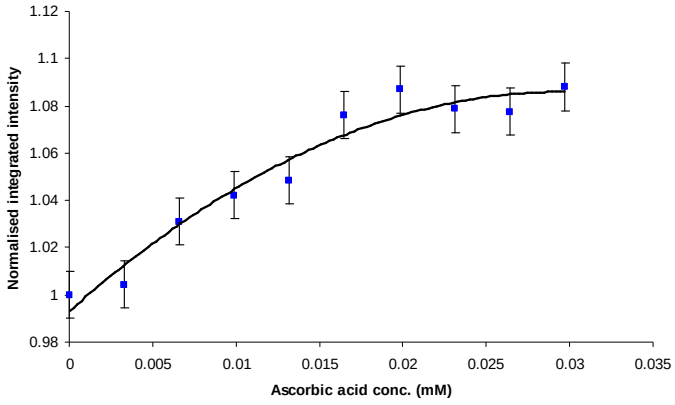

Figure 7.3. Integrated intensity for 1-PSA with increasing ascorbic acid concentration.

Fluorescence lifetimes for 1-PSA were measured for increasing concentration of ascorbic acid in aqueous solution, as described in the previous experiment. The fluorescence lifetime increases with increasing concentration of ascorbic acid. The results are consistent with the steady state measurement i.e. the fluorescence lifetime increases and then reaches a plateau value. The ascorbic acid concentration plateau value is approximately consistent with the value recorded from the steady-state results. The sample was measured again after 24 hours, and there was a measurable decrease in the fluorescence lifetime. This is likely to be as a result of oxygen redissolving into the aqueous sample. Results are shown in figure 7.4.

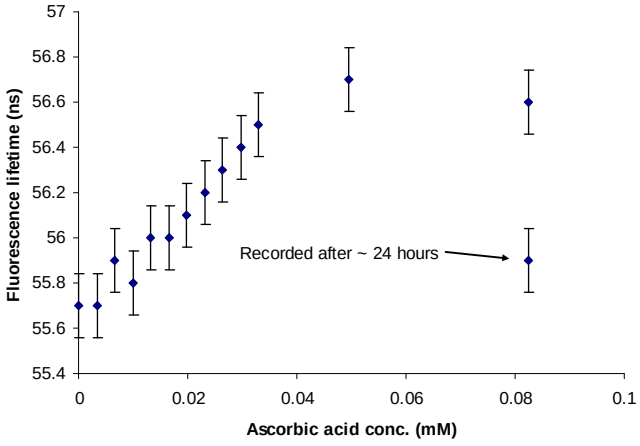

Figure 7.4. Fluorescence lifetime changes with Ascorbic acid concentration.

7.3.1 Sol-gels

Sol-gels were formed using excess H_2O, and aged for five days, as previously described. The oxygen probe 1-PSA was then introduced to the sol, and allowed to gel.

The initial fluorescence lifetime was measured on a sample with zero ascorbic acid added. The fluorescence lifetime recorded for this sample was 59.20 ± 0.12 ns, which is considerably higher than the fluorescence lifetime recorded for the aqueous sample recorded with zero ascorbic acid (55.70 ns). The fluorescence decay for 1-PSA entrapped in a sol-gel nano pore is shown in figure 7.5. The decay was measured 24 hours after the 1-PSA was added to the sol and the gel point was reached. The fluorescence decay for 1-PSA in aqueous solution is also shown for comparison. Both decays were recorded at zero ascorbic acid concentration

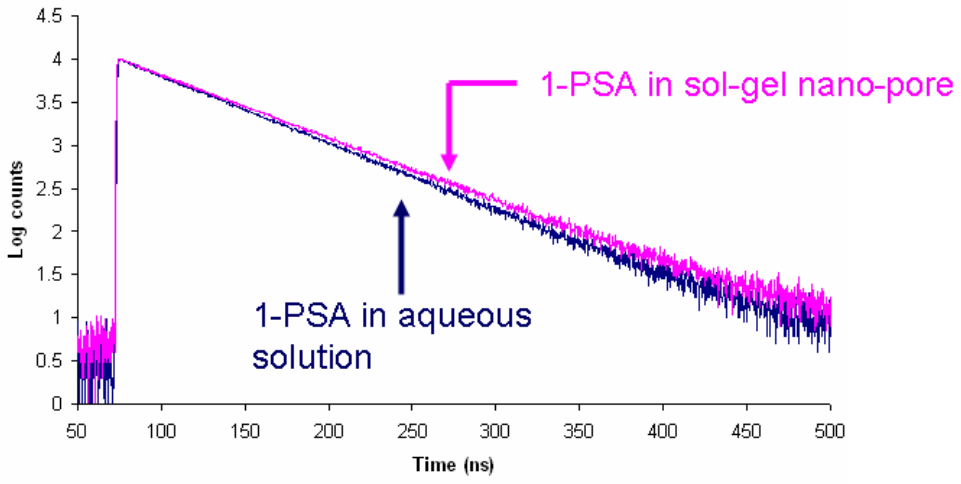

Figure 7.5. Fluorescence decay of entrapped 1-PSA in sol-gel nano-pore and in aqueous solution at zero ascorbic acid concentration

Several samples were prepared with an increasing concentration of ascorbic acid and the fluorescence lifetime of 1-PSA measured using time-correlated single photon counting.

The measurements were recorded 24 hours after the introduction of the probe and the sol-to gel process had gone to completion. The fluorescence lifetimes are plotted against increasing ascorbic acid concentration, as shown in figure 7.6.

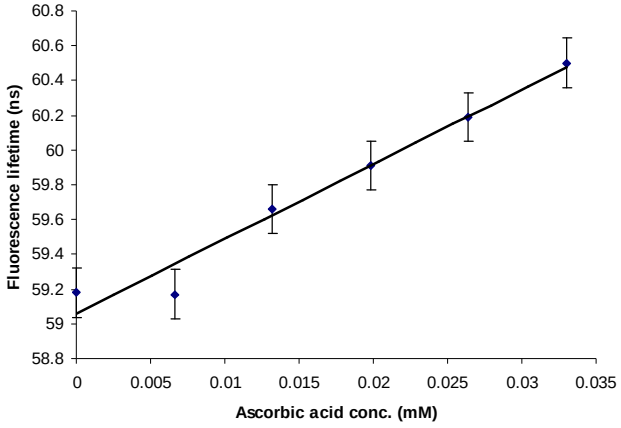

Figure 7.6. Fluorescence lifetime of 1-PSA entrapped in sol-gel nano-pores plotted against increasing ascorbic acid concentration.

There is a linear increase in the fluorescence lifetime of 1-PSA with increasing concentration of ascorbic acid. The results suggest that ascorbic acid is retarding the quenching effect of oxygen and thus the fluorophore remains in the excited state for a longer period. Furthermore, the increase in fluorescence lifetime upon encapsulation, in sol-gel nano-pores, suggests that entrapped fluorophore is somewhat protected from the negative effects of oxygen in comparison to the fluorophore in solution.

7.4 Summary

In this chapter the ability of the oxygen scavenger ascorbic acid to remove oxygen and as result increase fluorescence intensity and lifetime has been demonstrated. The ability to remove oxygen and stabilise fluorophores has benefits in the imaging and time-resolved

imaging of single molecules. However, as oxygen is also an effective quencher of the triplet state, the best results for single molecule stability will be achieved by the removal of oxygen and the addition of an alternative triplet state quencher [144].

Single-molecule fluorescence imaging and spectroscopy can provide previously unattainable data on elementary biological processes. The ability to encapsulate proteins of interest in silica sol-gel nano-pores, allows for study at its near natural state. The ability to couple this immobilisation technique with oxygen scavengers will allow for single molecule study for an extended time period, which was previously limited by the fluorophore's properties.

8

8. Conclusions and future work

8.1. Conclusions

The application of fluorescence spectroscopy has been demonstrated to the study of proteins and the development and application of protein entrapment in silica sol-gels to both ensemble and single-protein fluorescence measurement.

The amino acid phenylalanine was studied in detail using TCSPC. For a pH range of 1–11, there is evidence for a biexponential rather than a monoexponential decay, whereas at pH 13, only a monoexponential decay is present. These results are in contradiction to previous studies where monoexponential decays have been reported. However, this is somewhat surprising since the rotamer model for tyrosine and tryptophan photophysics is now widely accepted, but the existence of rotamers in phenylalanine has hitherto lacked supporting evidence because of its apparent monoexponential decay in solution. The results, presented in this thesis, provide direct evidence for the prescence of two phenylalanine rotamers in solution, which is consistent with results seen for the other two fluorescent amino acids, tyrosine and tryptophan.

The application of the fluorescent probe, 6-propionyl-2-(N,N-dimethylamino)naphthalene (PRODAN), to the study of TMOS sol-gel preparation and aging was investigated. The sensitivity of the fluorescent probe to polarity provided an approach to study and optimise changes in the sol–gel processes. The ability of PRODAN to report on the internal sol-gel

pores has the advantage that it reports on the solvent polarity of the environment where the protein will be localised.

The improvement provided through the study and optimisation of the sol-gel process was demonstrated by the encapsulation of the trimeric form of allophycocyanin for extended time periods in a monolith sol gel. Previous attempts at the encapsulation of this environment sensitive form have been unsuccessful, even when maintaining neutral pH either before or after gelation, presumably due to the protein's extreme sensitivity (through such mechanisms as disrupted hydrogen bonding) to the vicinal solvents and pH changes generated, resulting in dissociation to the monomeric form.

Spin coating of the improved sol allowed for the detection of trimeric allophycocyanin down to the single molecule level, thus obviating the common practice of covalent binding in order to stabilize this protein. To the best of my knowledge this is the first report on a single protein aggregating and deaggregating in a sol-gel nanopore.

Also, in the work presented here the effect of adding oxygen scavengers to solution and sol gel nanopores was investigated for possible application to the stabilization of single molecules allowing study for extended time periods.

The effect of ascorbic acid was investigated using the long lifetime fluorophore 1-Pyrene Sulphonic acid. The results showed that the fluorescence intensity and fluorescence lifetime of the fluorophore increased with increasing concentration of the scavenger. The results for the sol-gel showed that the gels provide protection to the quenching effect of oxygen, most likely as a result of restricted diffusion. However, the fluorescence lifetimes were further enhanced with the addition of ascorbic acid. The results illustrate the potential

of applying these oxygen limiting techniques to single molecule fluorescence where the presence of oxygen is most pronounced.

8.2 Future work

One of the major limitations of single molecule fluorescence is photobleaching as a result of interaction with molecular oxygen and intersystem crossing to a triplet state. Future work would include incorporating oxygen scavenging techniques to remove oxygen and introduce triplet-state quenchers in order to stabilise single-proteins within sol-gel nano-pores, allowing for time-resolved measurement. Another area of my research would be the application of metal surface plasmon techniques for fluorescence enhancement of proteins entrapped within silica sol-gel nano-pores. In addition to fluorescence being quenched on metal surfaces it can also be enhanced at the right spacing and this provides a potential means of overcoming the bleaching of single dye molecules. This should extend the use of single-molecule fluorescence techniques to the study of biomolecular function at the most fundamental level using near-field and confocal microscopy.

The porous nature of silica sol-gels offers the advantage that entrapped species remain accessible to and can interact with external chemical species or analytes of interest by permeation. This feature of silica sol-gels could be utilised for development of fluorescence lifetime assays within sol-gel nanometre size pores at ensemble, and further downstream to single-molecule level. Future work would be to demonstrate change in entrapped protein fluorescence as a result of interaction with analytes introduced through the porous network, with the ultimate goal of being able to sense metabolites such as glucose.

References

1. J.R. Lakowicz, Topics in Fluorescence Spectroscopy, *Volume 4: Probe Design and Chemical Sensing* edited by J. R. Lakowicz, (Plenum Press, New York) 1995.

2. O.J. Rolinski, A. Martin, and D.J.S. Birch, Human serum albumin and quercetin interactions monitored by time-resolved fluorescence: evidence for enhanced discrete rotamer conformations, *Journal of Biomedical Optics*, 2007. 12(3).

3. J.D. Brennan, Using intrinsic fluorescence to investigate proteins entrapped in sol-gel derived materials, *Applied Spectroscopy*, 1999. 53(3): p. 106A-121A.

4. A. Smith, Protein misfolding, *Nature*, 2003. 426(6968): p. 883-883.

5. S. Weiss, Measuring conformational dynamics of biomolecules by single molecule fluorescence spectroscopy, *Nature Structural Biology*, 2000. 7(9): p. 724-729.

6. Sir J.F.W. Herschel, On a case of superficial colour presented by a homogeneous liquid internally colourless, *Philiosophical Translation of the Royal Society of London*, 1845. 135: p. 143-145.

7. J.B. Birks, Photophysics of aromatic molecules (John Wiley & Sons Ltd., New York), 1970.

8. G.G. Stokes, On the change of refrangibility of light, *Philiosophical Translation of the Royal Society of London*, 1852. 142: p. 463.

9. M. Kasha, Characterisation of electronic transitions in complex molecules, *Discussions Faraday Society*, 1950. 9: p. 14-19.

10. J.R. Lakowicz, Principles of Fluorescence Spectroscopy, second edition, (Kluwer Academic/Plenum, New York),1999.

11. H. Kautsky, Quenching of luminescence by oxygen, *Transactions of the Faraday Society*, 1939. 35: p. 216-219.

12. D.J.S. Birch, and R.E. Imhof, Time-Domain Fluorescence Using Time-Correlated Single Photon Counting. *Topics in Fluorescence Spectroscopy, Volume 1: Techniques* edited by J. R. Lakowicz, (Plenum Press, New York), 1991: p. 1-95.

13. H. Szmacinski, and J.R. Lakowicz, Lifetime-Based Sensing, *Topics in Fluorescence Spectroscopy, Volume 4: Probe Design and Chemical Sensing* edited by J. R. Lakowicz, (Plenum Press, New York) 1995: p. 295-329.

14. R.F. Steiner, Fluorescence Anisotropy: Theory and applications, *Topics in Fluorescence Spectroscopy, Volume 2: Principles* edited by J. R. Lakowicz, (Plenum Press, New York) 1991: p. 1-52.

15. L. Stryer, Fluorescence energy-transfer as a spectroscopic ruler, *Annual Review of Biochemistry*, 1978. 47: p. 819-846.

16. L.M. Bollinger, and R.E. Thomas, Measurement of the time-dependence of scintillation intensity by a delayed-coincidence method, *Review of Scientific Instruments*, 1961. 32: p. 1044.

17. G. Hungerford, and D.J.S. Birch, Single-photon timing detectors for fluorescence lifetime spectroscopy, *Measurement Science & Technology*,1996. 7(2): p. 121-135.

18. D.V. O'Connor, and D. Phillips, Time-correlated Single-Photon Counting, (Academic Press, London.),1984.

19. P.R. Bevington, Data Reduction and Error Analysis for the Physical Sciences, (McGraw-Hill, New York.),1969.

20. M. Minsky, Memoir on inventing the confocal scanning microscope, *Scanning*, 1988. 10(4): p. 128-138.

21. K.R. Spring, Detectors for Fluorescence Microscopy, Methods in Cellular Imaging, edited by A. Periasamy (Oxford University Press, New York), 2001. p. 40-52.

22. J.B. Pawley (ed), Handbook of Biological Confocal Microscopy 2nd edn (New York: Plenum). 1995.

23. R.H. Webb, Confocal optical microscopy, *Reports on Progress in Physics*, 1996. 59(3): p. 427-471.

24. S. J. Wright, and D.J. Wright, Introduction to Confocal Microscopy. B. Matsumoto (ed.), Cell Biological Applications of Confocal Microscopy, in Methods in Cell Biology. New York: Academic Press, London, 2002. 70: p. 1-85.

25. M. Ebelmen, Sur les combinaisons des acides borique et silicique avec les ethers, *Annales des Chimie et des Physique* (1846). 16: p. 129.

26. M. Ebelmen, Sur l'hyalite artificielle et l'hydrophane, *Les Comptes rendus de l'Académie des sciences*, (1847). 25: p. 854.

27. T. Graham, On the properties of silicic acid and other analogous colloidal substances, J*ournal of the Chemical Society*, (1864). 17: p. 318

28. C. J. Brinker, and G.W. Scherer, Sol-Gel Science: The Physics and Chemistry of Sol-Gel Processing. (Academic Press, Inc.: New York). 1990.

29. P.C. Carman, Constitution of colloidal silica, *Transactions of the Faraday Society*, (1940). 36: p. 964.

30. R.K. Iler, The chemistry of silica .(John Wiley & Sons Ltd., New York), 1955.

31. D.J.S. Birch, C.D. Geddes, J. Karolin, R. Leishman, and O.J. Rolinski, Fluorescence nanometrology in sol-gels, in *Fluorescence Spectroscopy, Imaging and Probes*, edited by R.Kraayenhof, A. J. W. G. Visser, and H. C. Gerritsen (Springer, new York) 2002: p. 69-84.

32. A.J. Vega, and G.W. Scherer, Study of structural evolution of silica-gel using ^{1}H and ^{29}Si NMR, *Journal of Non-Crystalline Solids*, 1989. 111(2-3): p. 153-166.

33. T.W. Zerda, I. Artaki, and J. Jonas, Study of polymerization processes in acid and base catalyzed silica sol-gels, *Journal of Non-Crystalline Solids*, 1986. 81(3): p. 365-379.

34. G. Orcel, L. L. Hench, I. Artaki, J. Jonas, and T.W. Zerda , Effect of formamide additive on the chemistry of silica sol-gels II. Gel structure, *Journal of Non-Crystalline Solids*, 1988. 105(3): p. 223-231.

35. Z. Z.Vysotskii, and D.N. Strazhesko, in Adsorption and Absorbents edited by D.N. Strazhesko (Wiley, New york), 1973. p. 72-86.

36. F. Moore, The Mechanism of Moisture Movement in Clays with Particular Reference to Drying: A Concise Review, *Transactions and Journal of British Ceramic Society*, 1961. 60: p. 517-539.

37. H.H. Macey, Clay-water relationships and the internal mechanisms of drying, *Transactions and Journal of British Ceramic Society*, 1942. 41: p. 73-121.

38. N.H. Ceaglske, and O.A. Hougen, Drying Granular Solids, *Industrial & Engineering Chemistry*, 1937. 29: p. 805-813.

39. M. Fortes, and M.R. Okos, Drying theories: their bases and limitations as applied to food and grains, in *Advances in Drying* edited by A.S Mujumdar (Hemisphere, New York), 1980. 1: p. 119-154.

40. D.E. Bornside, C.W. Macosko, and L.E. Scriven, On the modeling of spin coating, *Journal of Imaging Technology*, 1987. 13(4): p. 122-130.

41. C.J. Brinker, A.J. Hurd, and K.J. Ward, in U*ltrastructure Processing of Advanced Ceramics* edited by J.D. Mackenzie, and D.R. Ulrich, (Wiley, New york), 1988: p. 223-240

42. L.L. Hench, and J.K. West, The Sol-Gel Process, *Chemical Reviews*, 1990. 90(1): p. 33-72.

43. H. Schroeder, Oxide Layers Deposited from Organic Solutions, in *Physics of Thin Films* edited by G. Hass and R. E. Thun, (Academic Press, New York), 1969. p. 87-141.

44. I. Strawbridge, and P.F. James, Thin silica films prepared by dip coating, *Journal of Non-Crystalline Solids*, 1986. 82(1-3): p. 366-372.

45. I. Strawbridge, and P.F. James, The factors affecting the thickness of sol-gel derived silica coatings prepared by dipping, *Journal of Non-Crystalline Solids*, 1986. 86(3): p. 381-393.

46. R.L. Aelion, A. Loebel, and F. Eirich, Hydrolysis of Ethyl Silicate, *Journal of the American Chemical Society*, 1950. 72: p. 5705-5712.

47. S. Braun, S. Rappoport, R. Zusman, D. Avnir, and M.Ottolenghi, Biochemically active sol-gel glasses: the trapping of enzymes, *Materials Letters*, 1990. 10(1-2): p. 1-5.

48. P. Debye, and J.O. Edwards, A Note on the Phosphorescence of Proteins, *Science*, 1952. 116: p. 143-144.

49. G. Weber, Rotational Brownian Motion and Polarization of the Fluorescence of Solutions, *Advances in Protein Chemistry*, 1953. 8: p. 415-459

50. D.E. Duggan, and S. Udenfriend, The spectrophotofluormetric determination of Tryptophan in Plasma and of Tryptophan and Tyrosine in Protein Hydrolysates, *Journal of Biological Chemistry*, 1956. 223: p. 313-319.

51. S. V. Konev, Fluorescence and Phosphorescence of Proteins and Nucleic Acids. (Plenum Press, New York), 1967.

52. A. P. Demchenko, Ultraviolet Spectroscopy of Proteins. (Springer-Verlag, Berlin), 1986.

53. R. F. Chen, Fluorescence quantum yields of tryptophan and tyrosine, *Analytical Letters*, 1967. 1: p. 35-42.

54. E. A. Permyakov, Luminescent Spectroscopy of Proteins. (CRC Press, Boca Raton, Fl), 1993.

55. R.W. Ricci, Deuterium-Isotope effect on the Fluorescence Yields and Lifetimes of Indole derivatives- including Tryptophan and Tryptamine, *Photochemistry and Photobiology*, 1970. 12(1): p. 67-75.

56. R. McGuire, and I. Feldman, The Quenching of Tyrosine and Tryptophan Fluorescence by H_2O and D_2O, *Photochemistry and Photobiology*, 1973. 18(2): p. 119-124.

57. W.B. De Lauder, and P. Wahl, pH dependence of the fluorescence decay of tryptophan, *Biochemistry*, 1970. 9(13): p. 2750-2754.

58. A. Rzeska, K. Stachowiak, J. Malicka, L. Łankiewicz, and W. Wiczk Photophysics of phenylalanine analogues - Part 1. Constrained analogues of phenylalanine modified at phenyl ring, *Journal of Photochemistry and Photobiology A: Chemistry*, 2000. 133(1-2): p. 33-38.

59. C.D. McGuinness, A.M. Macmillan, K. Sagoo, D. McLoskey, and D.J.S. Birch Excitation of fluorescence decay using a 265 nm pulsed light-emitting diode: Evidence for aqueous phenylalanine rotamers, *Applied Physics Letters*, 2006. 89(6): 063901: p. 1-3.

60. A.M. Macmillan, C.D. McGuinness, K. Sagoo, D. McLoskey, J. C. Pickup, and D.J.S. Birch, Effect of pH on aqueous phenylalanine studied using a 265-nm pulsed light-emitting diode, in *Fluorescence Methods and Applications: Spectroscopy, Imaging, and Probes*, 2008. p. 300-304.

61. C.D. McGuinness, K. Sagoo, D. McLoskey, and D.J.S. Birch, Selective excitation of tryptophan fluorescence decay in proteins using a subnanosecond 295 nm light-emitting diode and time-correlated single-photon counting, *Applied Physics Letters*, 2005. 86(26): 261911: p. 1-3.

62. C.D. McGuinness, K. Sagoo, D. McLoskey, and D.J.S. Birch, A new sub-nanosecond LED at 280 nm: application to protein fluorescence, *Measurement Science & Technology*, 2004. 15(11): p. L19-L22.

63. S. Nakamura, InGaN-based violet laser diodes, *Semiconductor Science and Technology*, 1999. 14(6): p. R27-R40.

64. A.A. Allerman, M.H. Crawford, A.J. Fischer, K.H.A. Bogart, S.R. Lee, D.M. Follstaedt, P.P. Provencio, and D. D. Koleske , Growth and design of deep-UV (240-290 nm) light emitting diodes using AlGaN alloys, *Journal of Crystal Growth*, 2004. 272(1-4): p. 227-241.

65. D.J.S. Birch, and R.E. Imhof, Coaxial Nanosecond Flashlamp, *Review of Scientific Instruments*, 1981. 52(8): p. 1206-1212.

66. M. Shatalov, A. Chitnis, V. Mandavilli, R. Pachipulusu, J.P. Zhang, V. Adivarahan, S. Wu, G. Simin, M. Asif Khan, G. Tamulaitis, A. Sereika, I. Yilmaz, M.S. Shur, and R. Gaska, Time-resolved electroluminescence of AlGaN-based light-emitting diodes with emission at 285 nm, *Applied Physics Letters*, 2003. 82(2): p. 167-169.

67. M.R. Chance, Unfolding of apomyoglobin examined by synchrotron footprinting, *Biochemical and Biophysical Research Communications*, 2001. 287(3): p. 614-621.

68. J.P. Duneau, N. Garnier, G. Cremel, G. Nulans, P. Hubert, D. Genest, M. Vincent, J. Gallay, and M. Genest, Time resolved fluorescence properties of phenylalanine in different environments. Comparison with molecular dynamics simulation, *Biophysical Chemistry*, 1998. 73(1-2): p. 109-119.

69. A.G. Szabo, and D.M. Rayner, Fluorescence Decay of Tryptophan Conformers in Aqueous-solution, *Journal of the American Chemical Society*, 1980. 102(2): p. 554-563.

70. P. Gauduchon, and P. Wahl, Pulse fluorimetry of tyrosyl peptides, *Biophysical Chemistry*, 1978. 8(1): p. 87-104.

71. A.H.A. Clayton, and W.H. Sawyer, Tryptophan Rotamer Distributions in Amphipathic Peptides at a Lipid Surface, *Biophysical Journal*, 1999. 76(6): p. 3235-3242.

72. F.W.J. Teale, and G. Weber, Ultraviolet fluorescence of the aromatic amino acids, *Journal of biochemistry*, 1957. 65: p. 476-482.

73. W.S. VanScyoc, and M.A. Shea, Phenylalanine fluorescence studies of calcium binding to N-domain fragments of Paramecium calmodulin mutants show increased calcium affinity correlates with increased disorder, *Protein Science*, 2001. 10(9): p. 1758-1768.

74. W.S. VanScyoc, B.R. Sorensen, E. Rusinova, W.R. Laws, J.B.A. Ross, and M.A Shea, Calcium binding to calmodulin mutants monitored by domain-specific intrinsic phenylalanine and tyrosine fluorescence, *Biophysical Journal*, 2002. 83(5): p. 2767-2780.

75. E.A. Permyakov, E.A. Burstein, Y. Sawada, and Y. Yamazaki, Luminescence of phenylalanine residues in superoxide dismutase from green pea, *Biochimica Et Biophysica Acta*, 1977. 491(1): p. 149-154.

76. L.C. Snoek, E.G. Robertson, R.T. Kroemer, and J. P. Simons, Conformational landscapes in amino acids: infrared and ultraviolet ion-dip spectroscopy of phenylalanine in the gas phase, *Chemical Physics Letters*, 2000. 321(1-2): p. 49-56.

77. S. J. Martinez, J.C. Alfano, and D.H. Levy, The electronic spectroscopy of the amino acids tyrosine and phenylalanine in a supersonic jet, *Journal of Molecular Spectroscopy*, 1992. 156(2): p. 421-430.

78. T. Hashimoto, Y. Takasu, Y. Yamada, and T. Ebata, Anomalous conformer dependent S_1 lifetime of L-phenylalanine, *Chemical Physics Letters*, 2006. 421(1-3): p. 227-231.

79. L.A. Philips, S.P. Webb, and S.J. Martinez, Time-resolved spectroscopy of tryptophan conformers in a supersonic jet, *Journal of the American Chemical Society*, 1988. 110(5): p. 1352-1355.

80. S. Ullrich, T. Schultz, M.Z. Zgierski, and A. Stolow, Electronic relaxation dynamics in DNA and RNA bases studied by time-resolved photoelectron spectroscopy, *Physical Chemistry Chemical Physics*, 2004. 6(10): p. 2796-2801.

81. J.W. Hager, D.R. Demmer, and S.C. Wallace, Electronic Spectra of Jet-Cooled Indoles: Evidence for the ^1L_a State, *Journal of Physical Chemistry*, 1987. 91(6): p. 1375-1382.

82. E. Leroy, H. Lami, and G. Laustriat, Fluorescence lifetime and quantum yield of phenylalanine aqueous solutions: temperature and concentration effects, *Photochemistry and Photobiology*, 1971. 13(5): p. 411-421.

83. J. Feitelson, Environmental effects on fluorescence of Tryptophan and other Indole derivatives, *Israel Journal of Chemistry*, 1970. 8(2): p. 241.

84. E.A. Burshtein, and E.P. Busel, Ways of deactivating excited state of Indole and its derivatives in aqueous solutions – Luminescence of Tryptophane in Alkaline medium at room temperature, *Optics and Spectroscopy-USSR*, 1970. 29(6): p. 580.

85. T.L. Bushueva, E.P. Busel, and E.A. Burshtein, Interaction of protein functional groups with Indole chromophore .3. Amine, Amide, and Thiol-groups, *Studia Biophysica*, 1975. 52(1): p. 41-52.

86. W. Altekar, The quenching of the tryptophyl and tyrosyl fluorescence of proteins by cesium ion, *FEBS Letters*, 1974. 49(2): p. 208-211.

87. G.A. Casay, D.B. Shealy, and G. Patonay, Near-Infrared Fluorescence Probes, *Topics in Fluorescence Spectroscopy, Volume 4: Probe Design and Chemical Sensing* edited by J. R. Lakowicz, (Plenum Press, New York)1995: p. 183-217.

88. J.N. Demas, and B.A. DeGraff, Design and Applications of Highly Luminescent Transition Metal Complexes, *Topics in Fluorescence Spectroscopy, Volume 4: Probe Design and Chemical Sensing* edited by J. R. Lakowicz, (Plenum Press, New York) 1995: p. 71-105.

89. W. Rettig, and R. Lapouyade, Fluorescent Probes Based on Twisted Intramolecular Charge Transfer (TICT) states and Other Adiabatic Photoreactions, *Topics in Fluorescence Spectroscopy, Volume 4: Probe Design and Chemical Sensing* edited by J. R. Lakowicz, (Plenum Press, New York) 1995: p. 109-141.

90. S.S. Bag, Y. Saito, K. Hanawa, S. Kodate, I. Suzuka, and I. Saito, Intelligent fluorescent nucleoside in sensing cytosine base: Importance of hydrophobic nature of perylene fluorophore, *Bioorganic & Medicinal Chemistry Letters*, 2006 16(24): p. 6338-6341.

91. J.L. Pozzo, L. Fuchtjohann , A. Ferraro , O. Provot, H. Bouas-Laurent , and J. P. Desvergne, Excimer fluorescence of a new bisanthracene as probe of viscosity in polysiloxanes, *Polycyclic Aromatic Compounds*, 2001. 18(3): p. 293-306.

92. I.D. Figueroa, M. El Baraka, E. Quiñones, O. Rosario, and M. Deumié, A fluorescent temperature probe based on the association between the excited states of 4-(N,N-dimethylamino)benzonitrile and β-cyclodextrin, *Analytical Chemistry*, 1998. 70(18): p. 3974-3977.

93. M. Kusube, N. Tamai, H. Matsuki, and S. Kaneshina, Pressure-induced phase transitions of lipid bilayers observed by fluorescent probes Prodan and Laurdan, *Biophysical Chemistry*, 2005. 117(3): p. 199-206.

94. G. Weber, and F.J. Farris, Synthesis and spectral properties of a hydrophobic fluorescent probe: 6-propionyl-2-(dimethylamino)naphthalene, *Biochemistry*, 1979. 18(14): p. 3075-3078.

95. D.J. Cowley, Protein structure: Polar pocket with nonpolar lining, *Nature*, 1986. 319(6048): p. 14-14.

96. F.V. Bright, T.L. Keimig, and L.B. McGown, Thermodynamic binding parameters evaluated by using Phase-Resolved Fluorescence Spectrometry, *Analytica Chimica Acta*, 1985. 175(SEP): p. 189-201.

97. P.M. Torgerson, H.G. Drickamer, and G. Weber, Inclusion Complexes of Poly-Beta-Cyclodextrin – Model for pressure effects upon ligand-protein complexes, *Biochemistry*, 1979. 18(14): p. 3079-3083.

98. A.M. Rollinson, and H.G. Drickamer, High pressure study of luminescence from intramolecular CT compounds, *Journal of Chemical Physics*, 1980. 73(12): p. 5981-5996.

99. C.F. Chapman, R.S. Fee, and M. Maroncelli, Solvation dynamics in N-methylamides, *Journal of Physical Chemistry*, 1990. 94(12): p. 4929-4935.

100. C.F. Chapman and M. Maroncelli, Fluorescence studies of solvation and solvation dynamics in ionic solutions, *Journal of Physical Chemistry*, 1991. 95(23): p. 9095-9114.

101. T.A. Betts, J. Zagrobelny, and F.V. Bright, Investigation of solute-fluid interactions in supercritical CF_3H: A multifrequency phase and modulation fluorescence study, *Journal of Supercritical Fluids*, 1992. 5(1): p. 48-54.

102. T.A. Betts, J. Zagrobelny, and F.V. Bright, Spectroscopic determination of solute-fluid cluster size in supercritical nitrogen oxide (N_2O), *Journal of the American Chemical Society*, 1992. 114(21): p. 8163-8171.

103. I. Gill, and A. Ballesteros, Encapsulation of biologicals within silicate, siloxane, and hybrid sol-gel polymers: An efficient and generic approach, *Journal of the American Chemical Society*, 1998. 120(34): p. 8587-8598.

104. R.B. Bhatia, C.J. Brinker, A.K. Gupta, and A.K. Singh, Aqueous sol-gel process for protein encapsulation, *Chemistry of Materials*, 2000. 12(8): p. 2434-2441.

105. J. Catalan, P. Perez, J. Laynez, and F.G. Blanco, Analysis of the solvent effect on the photophysics properties of 6-propionyl-2-(dimethylamino)naphthalene (PRODAN), *Journal of Fluorescence*, 1991. 1(4): p. 215-223.

106. F. Hussain, D.J.S. Birch, and J.C. Pickup, Glucose sensing based on the intrinsic fluorescence of sol-gel immobilized yeast hexokinase, *Analytical Biochemistry*, 2005. 339(1): p. 137-143.

107. J.R. Lakowicz, and G. Weber, Quenching of fluorescence by oxygen - Probe for structural fluctuations in macromolecules, *Biochemistry*, 1973. 12(21): p. 4161-4170.

108. J.R. Lakowicz, and G. Weber, Quenching of protein fluorescence by oxygen - Detection of structural fluctuations in proteins on nanosecond time scale, *Biochemistry*, 1973. 12(21): p. 4171-4179.

109. R. MacColl, and D. Guard-Friar, Phycobiliproteins, (CRC Press, Boca Raton, Florida),1987.

110. L.M. Ying, and X.S. Xie, Fluorescence spectroscopy, exciton dynamics, and photochemistry of single Allophycocyanin trimers, *Journal of Physical Chemistry B*, 1998. 102(50): p. 10399-10409.

111. D. Loos, M. Cotlet, F. De Schryver, S. Habuchi, and J. Hofkens, Single-molecule spectroscopy selectively probes donor and acceptor chromophores in the phycobiliprotein allophycocyanin, *Biophysical Journal*, 2004. 87(4): p. 2598-2608.

112. Z. Chen, D.L. Kaplan, K. Yang, J. Kumar, K.A. Marx, and S.K. Tripathy, Phycobiliproteins encapsulated in sol-gel glass, *Journal of Sol-Gel Science and Technology*, 1996. 7(1-2): p. 99-108.

113. R. MacColl, K. Csatorday, D.S. Berns, and E. Traeger, Chromophore interactions in allophycocyanin , *Biochemistry*, 1980. 19(12): p. 2817-2820.

114. M.L. Ferrer, F. del Monte, and D. Levy, A novel and simple alcohol-free sol-gel route for encapsulation of labile proteins, *Chemistry of Materials*, 2002. 14(9): p. 3619-3621.

115. C.D. McGuinness, A.M. Macmillan, J. Karolin, W.E. Smith, D. Graham, J.C. Pickup, and D.J.S. Birch, Single molecule level detection of allophycocyanin by surface enhanced resonance Raman scattering, *Analyst*, 2007. 132(7): p. 633-634.

116. X.S. Xie, and R.C. Dunn, Probing single-molecule dynamics, *Science*,1994. 265 (5170): p. 361-364.

117. H.P. Lu, and X.S. Xie, Single-molecule spectral fluctuations at room temperature, *Nature*, 1997. 385(6612): p. 143-146.

118. W.P. Ambrose, P.M. Goodwin, J. C. Martin, and R. A. Keller, Single molecule detection and photochemistry on a surface using near-field optical excitation, *Physical Review Letters*, 1994. 72(1): p. 160-163.

119. W.P. Ambrose, P.M. Goodwin, J. C. Martin, and R. A. Keller, Alterations of single-molecule Fluorescence lifetimes in near-field optical microscopy, *Science*, 1994. 265(5170): p. 364-367.

120. E. Betzig, and J.K. Trautman, Near-field optics - Microscopy, Spectroscopy, and Surface modification beyond the diffraction limit, *Science*, 1992. 257(5067): p. 189-195.

121. D.A. McL Smith, S.A. Williams, R.D. Miller and R.M. Hochstrasser, Near-field time-resolved fluorescence studies of poly(phenylmethyl silane) with sub-wavelength resolution, *Journal of fluorescence*, 1994. 4(2): p. 137-140.

122. J.K. Trautman, J.J. Macklin, L.E. Brus, and E. Betzig, Near-field spectroscopy of single molecules at room temperature, *Nature*, 1994. 369(6475): p. 40-42.

123. J.J. Macklin, J.K. Trautman, T.D. Harris, and L.E. Brus, Imaging and time-resolved spectroscopy of single molecules at an interface, *Science*, 1996. 272(5259): p. 255-258.

124. F. Vargas , O. Hollricher , O. Marti , G. de Schaetzen , and G. Tarrach, Influence of protective layers on the blinking of fluorescent single molecules observed by confocal microscopy and scanning near field optical microscopy, *Journal of Chemical Physics*, 2002. 117(2): p. 866-871.

125. S.M. Nie, and R.N. Zare, Optical detection of single molecules, *Annual Review of Biophysics and Biomolecular Structure*, 1997. 26: p. 567-596.

126. H. Heinzelmann, and D.W. Pohl, Scanning near-field optical microscopy, A*pplied Physics A - Materials Science & Processing*, 1994. 59(2): p. 89-101.

127. M.A. Bopp, A.J. Meixner, G. Tarrach, I. Zschokke-Gränacher, and L. Novotny, Direct imaging single molecule diffusion in a solid polymer host, *Chemical Physics Letters*, 1996. 263(6): p. 721-726.

128. I. Rasnik, S.A. McKinney, and T. Ha, Nonblinking and long-lasting single-molecule fluorescence imaging, *Nature Methods*, 2006. 3(11): p. 891-893.

129. J. C. Pickup, F. Hussain, N.D. Evans, and N. Sachedina, In vivo glucose monitoring: the clinical reality and the promise, *Biosensors & Bioelectronics*, 2005. 20(10): p. 1897-1902.

130. A. Cleary, A. Glidle, P.J.R. Laybourn, S. García-Blanco, S. Pellegrini, C. Helfter, G.S. Buller, J.S. Aitchison, and J.M. Cooper, Integrating optics and microfluidics for time-correlated single-photon counting in lab-on-a-chip devices, *Applied Physics Letters*, 2007. 91(7): p. 3.

131. D.J.S. Birch, A.S. Holmes, and M. Darbyshire, Intelligent sensor for metal ions based on fluorescence resonance energy transfer, *Measurement Science & Technology*, 1995. 6(2): p. 243-247.

132. O.J. Rolinski, and D.J.S. Birch, A fluorescence lifetime sensor for Cu(I) ions, *Measurement Science & Technology*, 1999. 10(2): p. 127-136.

133. D.J.S. Birch, A.S. Holmes, J.R. Gilchrist, R.E. Imhof, S.M. Al Alawi, and B. Nadolski, A multiplexed single-photon instrument for routine measurement of time-resolved fluorescence anisotropy, *Journal of Physics E: Scientific Instruments*, 1987. 20(4): p. 471-473.

134. S.A. Soper, H.L. Nutter, R.A. Keller, L.M. Davis, and E.B. Shera, The photophysical constants of several fluorescent dyes pertaining to ultrasensitive fluorescence spectroscopy, *Photochemistry and Photobiology*, 1993. 57(6): p. 972-977.

135. T. Schmidt, Datasheet: Photostability Data for Fluorescent Dyes, *Single Molecules*, 2001. 2: p. 217

136. W.E. Moerner, and D.P. Fromm, Methods of single-molecule fluorescence spectroscopy and microscopy, *Review of Scientific Instruments*, 2003. 74(8): p. 3597-3619.

137. F. Wilkinson, D.J. McGarvey, and A.F. Olea, Excited Triplet State Interactions with Molecular Oxygen: Influence of Charge Transfer on the Bimolecular Quenching Rate Constants and the Yields of Singlet Oxygen [O_2^*,$^1\Delta g$)] for Substituted Naphthalenes in Various Solvents, *Journal of Physical Chemistry*, 1994. 98(14): p. 3762-3769.

138. C. Eggeling, J. Widengren, R. Rigler, and C.A.M. Seidel, Photobleaching of fluorescent dyes under conditions used for single-molecule detection: Evidence of two-step photolysis, *Analytical Chemistry*, 1998. 70(13): p. 2651-2659.

139. H. Sies, and C.F.M. Menck, Singlet oxygen induced DNA damage, *Mutation Research*, 1992. 275(3-6): p. 367-375.

140. A.A. Earp, T. Rawling, J.B. Franklin, and G.B. Smith, Perylene dye photodegradation due to ketones and singlet oxygen, *Dyes and Pigments*, 2009, 84(1): p. 59-61.

141. M. Ahmad, M.D. Rahn, and T.A. King, Singlet oxygen and dye-triplet-state quenching in solid-state dye lasers consisting of Pyrromethene 567-doped poly(methyl methacrylate), *Applied Optics*, 1999. 38(30): p. 6337-6342.

142. G.J. Schütz, H.J. Gruber, H. Schindler, and T Schmidt, Fluorophores for single molecule microscopy, *Journal of Luminescence*, 1997. 72-74: p. 18-21.

143. J. Windengren, and R. Rigler, Mechanisms of photobleaching investigated by fluorescence correlation spectroscopy, *Bioimaging*, 1996. 4(3): p. 149-157.

144. C.G. Hubner, A. Renn, I. Renge, and U.P. Wild, Direct observation of the triplet lifetime quenching of single dye molecules by molecular oxygen, *Journal of Chemical Physics*, 2001. 115(21): p. 9619-9622.

145. L.A. Deschenes, and D.A. Vanden Bout, Single-molecule studies of heterogeneous dynamics in polymer melts near the class transition, *Science*, 2001. 292(5515): p. 255-258.

146. K.D.Weston , P.J. Carson , J. A.DeAro , and S. K. Burrato, Single-molecule detection fluorescence of surface-bound species in vacuum, *Chemical Physics Letters*, 1999. 308(1-2): p. 58-64.

147. C.E. Aitken, R.A. Marshall, and J.D. Pulglisi, An oxygen scavenging system for improvement of dye stability in single-molecule fluorescence experiments, *Biophysical Journal*, 2008. 94(5): p. 1826-1835.

148. J. Widengren, A. Chmyrov, C.Eggeling, P. A. Löfdahl, and C.A.M. Seidel, Strategies to improve photostabilities in ultrasensitive fluorescence spectroscopy, *Journal of Physical Chemistry A*, 2007. 111(3): p. 429-440.

149. P.S. Dittrich, and P. Schwille, Photobleaching and stabilization of fluorophores used for single-molecule analysis with one- and two-photon excitation, *Applied Physics B: Lasers and Optics*, 2001. 73(8): p. 829-837.

150. E. Miller, and D. Jozwik-Styczynska, The mechanism of pyrene fluorescence quenching by selective and nonselective quenchers during sol-gel transition, *Colloid and Polymer Science*, 2007. 285(14): p. 1561-1571.